



Vector trace cells in the subiculum of the hippocampal formation

Steven Poulter¹✉, Sang Ah Lee², James Dachtler¹, Thomas J. Wills^{3,4}✉ and Colin Lever^{1,4}✉

Successfully navigating in physical or semantic space requires a neural representation of allocentric (map-based) vectors to boundaries, objects and goals. Cognitive processes such as path-planning and imagination entail the recall of vector representations, but evidence of neuron-level memory for allocentric vectors has been lacking. Here, we describe a novel neuron type, vector trace cell (VTC), whose firing generates a new vector field when a cue is encountered and a ‘trace’ version of that field for hours after cue removal. VTCs are concentrated in subiculum, distal to CA1. Compared to non-trace cells, VTCs fire at further distances from cues and exhibit earlier-going shifts in preferred theta phase in response to newly introduced cues, which demonstrates a theta-linked neural substrate for memory encoding. VTCs suggest a vector-based model of computing spatial relationships between an agent and multiple spatial objects, or between different objects, freed from the constraints of direct perception of those objects.

Neurons in the hippocampal formation represent an organism's allocentric location and heading^{1–3}, and the fundamental coding underlying these spatial representations, for instance involving the theta oscillation, likely support planning, imagination and memory beyond the purely spatial domain^{6–9}. Spatial coding may be vector-based such that a neuron fires at a particular allocentric distance and direction from an environmental boundary or object^{10–14}, and path-planning and imagination often entail the recall of vector representations of environmental cues^{7,14–16}.

Here, we examined vector-based representations in the subiculum. The subiculum is a major output region of the hippocampal formation^{17–19}. The subiculum is known to contain vector representations¹¹, is implicated in memory retrieval^{20,21} and has recently been identified as likely the hippocampal component of the default mode network²². This suggests a wide role for subicular vector-based representations in directing navigation and memory-based cognition, consistent with models of spatial memory and imagery⁷.

Accordingly, we exposed rats to a range of cues differing in size, shape and sensory properties, and tested for memory-based responses in subicular neurons following cue removal.

Results

Cue-responsive cells: defining vector trace cells (VTCs) and non-trace cells. Figure 1a shows a schematic of the experimental manipulations. The dataset comprised only subicular cue-responsive neurons that showed spatial tuning to environmental boundaries¹¹ and inserted cues. Responsiveness to inserted cues was defined by the appearance of a new firing field (‘cue field’) in the cue trial (253 cells passed this criterion; Methods). We quantified the strength of memory-based firing in the region of the cue field in the post-cue trial using two measures: (1) a ‘trace score’, which measured the strength of firing in the cue-field region in the post-cue trial; and (2) an ‘overlap score’, which measured whether firing in the post-cue trial outside the wall field (termed the ‘post-cue field’) was spatially overlapping with the cue-field region. (Fig. 1b, right-most column,

and Fig. 1c; Methods). Together, the trace and overlap scores define a group of neurons that show memory-based firing persistence, specifically in the region of the cue field (firing hereafter referred to as the ‘trace field’). For further analysis, those neurons with trace score values ≥ 0.205 and overlap scores ≥ 0.380 were defined as showing trace responses, here termed VTCs (73 out of 253) (Fig. 1c and see Extended Data Fig. 1 for co-recorded examples of both cell types (VTCs and non-trace cells), where threshold values represent the 90th percentiles of populations of trace and overlap scores derived from spatially shuffled data (Methods)).

For vector coding to enable efficient navigation, it should be flexible and operate over a range of cue types and distances. Subiculum neurons were responsive to a range of different cue types (Fig. 1b, left column), and all cue types were capable of eliciting a memory-based response (Fig. 1d). Cue-responsive subiculum neurons are therefore capable of encoding allocentric vectors to a wide range of external cues, including both discrete objects and extended boundaries¹¹. A subset of cue-responsive cells were exposed to multiple cues during one experimental session. Non-trace cells demonstrated a significant tendency to not form memory traces in response to any cues presented (Extended Data Fig. 2a,b). Systematic assessment of VTC responses to multiple cues was rendered difficult by the proportionally lower sampling of VTCs in multiple-cue sessions and the long-lasting nature of trace responses (see below), which made cue responses to later cues difficult to discriminate from trace responses to earlier cues. However, evidence from the limited numbers of cells where multiple-cue responses are detectable suggests that VTCs were significantly likely to show a trace response to multiple cue types (Extended Data Fig. 2c,d).

VTCs exhibit longer and more variable vector distance tunings than non-trace cells. To quantify the spatial characteristics of both VTC and non-trace cell cue responses, we constructed vector-firing-rate maps that expressed cue-responsive and memory-based firing as a function of the distance and direction of the animal to the cue (Fig. 2a,b and Methods). The distance tunings

¹Psychology Department, Durham University, Durham, UK. ²Department of Bio and Brain Engineering, Korea Advanced Institute of Science and Technology, Daejeon, Republic of Korea. ³Department of Cell and Developmental Biology, UCL, London, UK. ⁴These authors contributed equally: Thomas J. Wills, Colin Lever. ✉e-mail: steven.poulter@durham.ac.uk; t.wills@ucl.ac.uk; colin.lever@durham.ac.uk

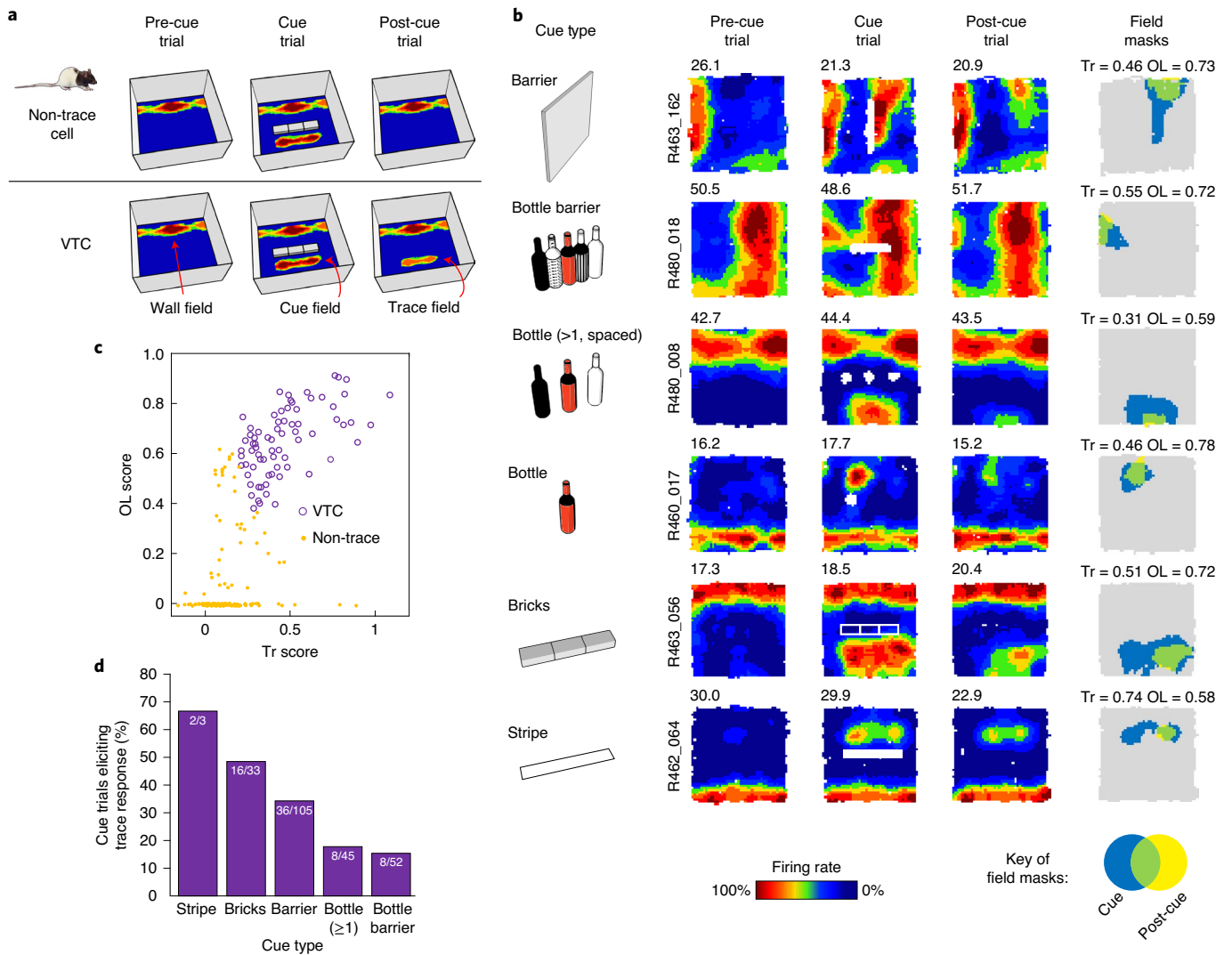


Fig. 1 | Vector trace responses to a range of cues. **a**, Schematic of the experimental procedure, including illustrative results. Rats foraged for food while neurons were recorded in the dorsal subiculum. Heatmaps show firing rates of a neuron as a function of the position of the rat (warmer colors indicate higher firing rates). Top: schematic of a non-trace vector cell responsive to insertion of a new cue (cue trial) but lacking a memory trace field in the post-cue trial. Bottom: a VTC whose cue-responsive firing field persists during the post-cue trial following cue removal. **b**, Six representative VTCs. Left: type of cue used. Middle: firing-rate maps, with the peak firing rate (Hz) at the top-left of each map, and rat and cell identifier numbers on the left of the maps. Each cell (row) forms a new firing field when the cue (white space or lines) is introduced (cue). Following cue removal (post-cue), cue-responsive firing field persists in the region of the cue field. Right: masks showing the cue-responsive field (blue), the post-cue field (yellow) and the overlap between both, indicative of a trace response (green). Trace (Tr) and overlap (OL) scores are shown above each plot. **c**, Scatter plot of trace and overlap scores for all cue-responsive neurons ($n = 73$ VTCs, $n = 180$ non-trace cells). VTCs are defined by combined above-threshold trace and overlap scores. **d**, Percentages of tested cue-responsive neurons categorized as VTCs for each cue type. Fractions overlaid on bars show the number of cue-responsive neurons recorded for cue type (denominator) and number of these neurons categorized as VTCs (numerator).

of VTC cue responses were much longer (VTCs = 18.8 ± 1.2 cm; non-trace = 12.4 ± 0.6 cm; Welch $t_{195} = 4.68$, $P < 0.0001$; Fig. 2c), and showed a much wider variance (F -test variance ratio = 2.47, $P < 0.001$) than those of non-trace cells. Differences between VTC and non-trace cells therefore also extend to the nature of their spatial firing in response to a cue.

Angular tunings (Fig. 2c, middle and bottom rows) of both cell types were not unimodally concentrated (Rayleigh test for uniformity: VTCs, $P = 0.95$; non-trace, $P = 0.17$). Non-trace angular tunings showed a significant departure from uniformity in the form of concentrated angular tunings at the cardinal compass directions (probably reflecting north–south and east–west cue orientations; $n = 132$, $U^2 = 0.31$, $P < 0.005$, Kuiper's $V = 2.48$, $P < 0.01$).

However, VTC angular tunings did not significantly depart from uniformity in VTCs ($n = 64$, $U^2 = 0.108$, $0.25 > P > 0.15$, Kuiper's $V = 1.479$, $P > 0.15$).

We also characterized the vector tunings of VTC trace fields in the post-cue trial and compared these to cue-field tunings in the cue trial (Fig. 2d,e). While the angular tunings of VTC fields were largely stable (mean angular difference between the cue and trace field = $6.6 \pm 3.2^\circ$, mean absolute angular difference = $19.5 \pm 2.7^\circ$), the distance tunings demonstrated a systematic increase between cue and post-cue trials, from 19.0 ± 1.2 cm in the cue field to 25.9 ± 1.7 cm in the trace field ($t_{63} = 6.395$, $P < 0.0001$; Fig. 2e, inset). Movements of the cue-responsive field between the cue and post-cue trial therefore uncovered a dissociation between the

components of vector tuning, whereby angular tuning remained stable while distance tuning systematically increased.

To further examine what determines the trace-field position in the post-cue trial, we tested whether trace-field location could be related to a pre-existing spatial structure in the firing of a cell, which is already present in the pre-cue trial. To do this, we calculated the correlations of spatial-bin firing rates across the pre- and post-cue trials, specifically within the cue- and post-cue fields. We found that although all such correlations were significantly greater than zero for VTCs, the correlations were not significantly greater than populations of correlations derived from spatially shuffled field positions (Extended Data Fig. 3). Therefore, the VTC trace-field position does not appear to be specifically related to pre-existing spatial firing structure in the pre-cue trial.

We also examined vector tunings for wall-responsive firing in the pre-cue trial (Extended Data Fig. 4). Angular tunings for wall-field and cue-field vectors were similarly stable across VTCs and non-trace cells (Extended Data Fig. 4b). The distance tunings of wall-field vectors in VTCs were longer and showed more variance than those of non-trace cells (Extended Data Fig. 4c). Distance tunings were longer for cue fields than wall fields in both cell types, but this was more pronounced in VTCs (Extended Data Fig. 4d).

Vector trace fields reflect memory, not responses to local cues.

Could VTC trace fields reflect perceptual responses to odor cues left behind by objects rather than memory? To rule out this possibility, a subset of VTCs (18%, 13 out of 72) in post-cue trials were subjected to the rotation of either the box and floor of the animal ('intra-box' cues) or room cues outside the box ('extra-box' cues). In all cases, VTC field location was concomitant with extra-box, not intra-box cues (Fig. 3). When presubicular head-direction cells were co-recorded with VTCs, head-direction-cell-preferred firing directions rotated in synchrony with VTCs (Fig. 3a, bottom row), which suggests that VTCs are coherently integrated into the overall hippocampal representation of the recording arena rather than responding to discrete local odor cues. These observations strongly argue that trace fields reflect mnemonic processing rather than responses to local cues (for example, odors) left behind by the removed cues.

Vector trace memory lasts for hours. To test how long VTC memory persists, a subset of VTCs were exposed to several post-cue trials in succession (Fig. 4a,b). Over 0.4–2.5 h (2–4 exposures), trace scores of VTCs decayed over time, but they were consistently significantly higher than those of non-trace cells (two-way analysis of variance (ANOVA) trace scores: exposure \times cell type; $F_{2,112} = 5.9$, $P = 0.004$; two-tailed post hoc simple main effects VTC versus non-trace: 0.4 h, $P < 0.001$; 1.3 h, $P < 0.001$; 2.5 h, $P = 0.042$; Fig. 4b).

These findings demonstrate that VTCs encode memories of cue location at hours-long timescales that would be highly likely to support adaptive spatial behavior. The temporal decay in trace strength may additionally signal how long ago a cue was encountered.

Proximodistal axis: vector trace cells are common in the distal subiculum but rare in the proximal subiculum.

The proximodistal anatomical axis is considered a major organizational feature of the subiculum based on patterns of connectivity and gene expression^{17–19}. The proximal subiculum is thought to support 'what?' memory while the distal subiculum supports 'where?' (allocentric) memory^{18,23}. However, in vivo electrophysiological evidence for proximodistal functional specialization is largely absent^{11,24}, consisting, at best, only of a gradient in mean firing rate and modest changes in spatial information content, for example^{25,26}. However, here, strikingly we found that VTCs are overwhelmingly found in the distal subiculum (distal VTCs constituting 69 out of 193 (36%), and proximal VTCs 3 out of 56 (5%), of cue-responsive cells ($n = 249$, $\chi^2(1) = 19.51$, $P = 0.00001$); for 4 out of 253 cells, a distal or proximal location could not be confidently assigned; Fig. 5), which strongly suggests that the distal subiculum has a specialized role in spatial memory.

As the scale of spatial representation is known to change along other anatomical axes in the broader hippocampal formation^{3,27}, it is possible that the longer and more variable vector distance tunings of VTCs compared to non-trace cells (Fig. 2c and Extended Data Fig. 2c) may be due to the concentration of VTCs in the distal, as opposed to the proximal, subiculum. However, differences between VTC and non-trace vector distance tunings remained robust even when considering only those cells in the distal subiculum (distance: VTCs = 19.3 ± 1.3 cm; non-trace = 13.7 ± 0.7 cm; Welch $t_{156} = 3.76$, $P = 0.0003$; variance: F -test ratio = 2.27, $P < 0.001$). Accordingly, these distance-tuning differences between VTCs and non-trace cells cannot be attributed to proximodistal variation in distance tuning.

Proximodistal axis: cue-responsive cells in the distal division of the subiculum fire at an earlier phase of theta than proximal cue-responsive cells.

Changes in spike timing with respect to the ongoing theta oscillation may modulate the function of hippocampal neurons in memory encoding and retrieval^{4,28–30}. We began by first asking whether the degree of theta modulation and preferred phase of cue-responsive neurons differed across the proximal and distal divisions of the subiculum in the baseline situation.

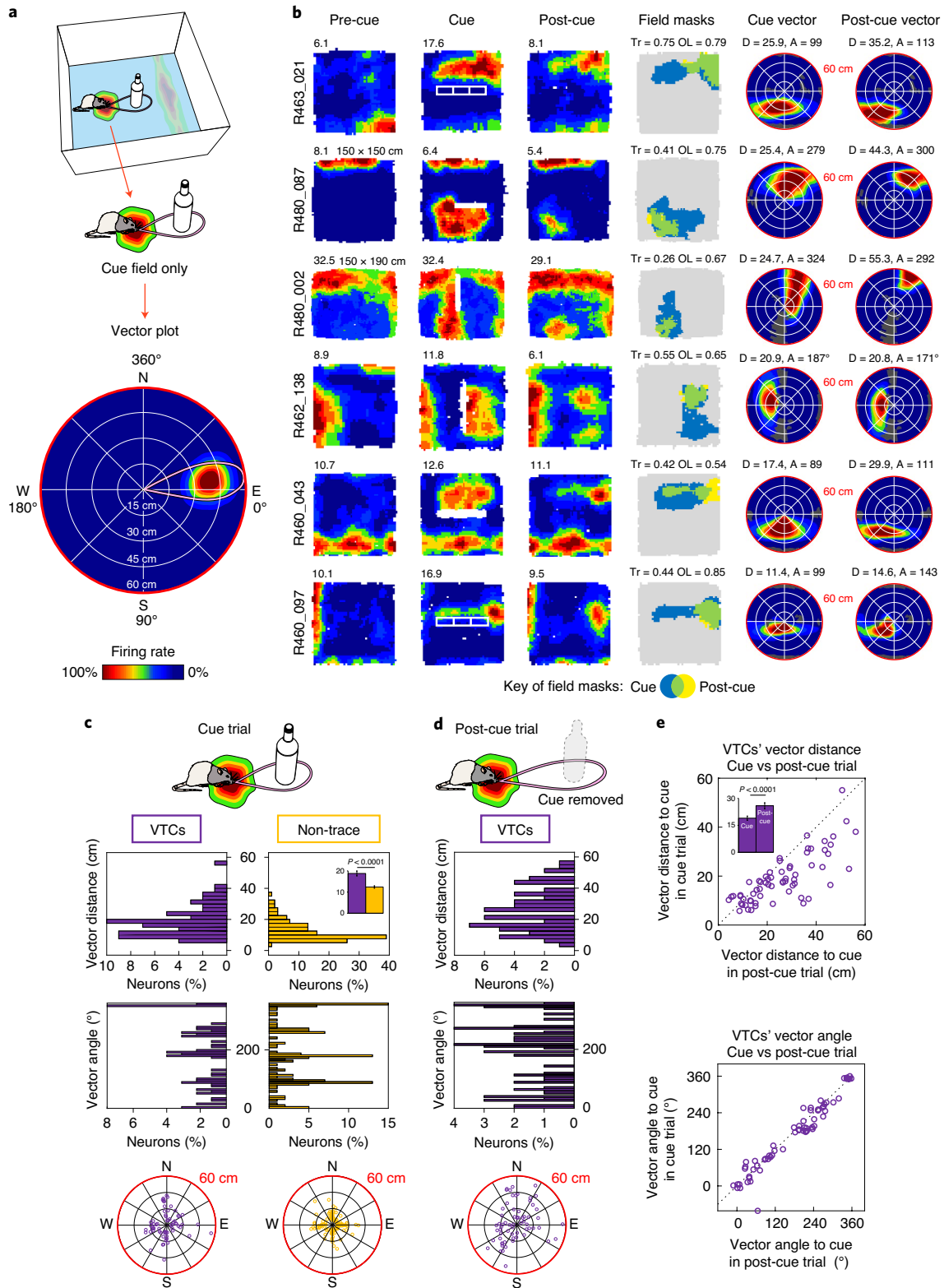
Theta modulation was higher in distal than proximal cue-responsive cells (Rayleigh r , pre-cue trial: distal ($n = 182$): 0.162 ± 0.006 ; proximal ($n = 45$): 0.137 ± 0.010 , $T_{225} = 2.03$, $P = 0.04$).

Fig. 2 | Vector field properties. **a**, Schematic illustrating the estimation of the cue vector from the cue field. Top: the firing of a cell generates a wall field and cue field. Middle: our analysis here focused on the cue field only. Bottom: a vector plot derived from the cue field, which shows the mean firing rate as a function of the displacement of the rat from the cue position. Concentric rings from the center to the circumference show 15-cm intervals used to represent the distance tuning of the cell; angles going clockwise (east = 0°) represent angular tuning. Thus, this example indicates the cell fires most strongly when a cue occurs ~22–30 cm away (distance tuning) east of the rat (angular tuning). **b**, Rate maps and cue vector plots for six representative VTCs. Conventions are as for Fig. 1 for first four columns. Non-standard box sizes are indicated above the pre-cue rate maps. The two columns on the far right show vector plots for cue field vectors in the cue trial (fifth column) and trace field vectors in the post-cue trial (sixth column). Vector plot conventions are as in **a** (bottom). 'D' and 'A' values above the vector plots give the peak of distance tunings (cm) and the angular tunings (degrees), respectively. Dark gray regions indicate unsampled bins. The distance tuning scale maximum is 0–60 cm (red circumference). **c**, Cue vectors estimated from cue-present trial (VTCs: $n = 64$; non-trace cells: $n = 132$). Top histogram: the distance tunings of VTCs have larger variance and longer distance in the vector tunings of VTCs than those of non-trace cells. The inset compares the mean \pm s.e.m. values for both cell types (two-tailed P value: Welch $t_{195} = 4.68$). Bottom histogram: the angular tunings of non-trace cells are clustered around the four cardinal directions. Polar plots (bottom) depict distributions of vectors (each small circle represents one cell; distance scale is 0–60 cm from the center to the circumference). **d**, The distribution of distance tunings (top histogram), angular tunings (bottom histogram) and vectors (polar plot) derived from trace fields in the post-cue trial. **e**, Scatterplots showing the changes in distance tunings (top) and angular tunings (bottom) between the cue and post-cue trial for VTCs ($n = 64$). The inset in the top plot compares the mean \pm s.e.m. values for the cue trial (left) and the post-cue trial (right) (two-tailed, paired P value: $t_{63} = 6.395$). Distance tunings are longer in the post-cue trial than the cue trial, whereas angular tunings are stable across the cue and post-cue trials.

When referencing the theta phase of all cells to distally recorded theta, distal cue-responsive cells fired at a considerably earlier phase of theta than proximal cue-responsive cells (Extended Data Fig. 5a,b): 59.4° ; pre-cue trial: distal = $178 \pm 3^\circ$, proximal = $238 \pm 9^\circ$; Watson-Williams $F_{1,225} = 68.50$, $P < 1 \times 10^{-12}$.

We asked whether this marked difference in theta-phase preference across proximal and distal divisions was specific to

cue-responsive cells or extended to other cell types. Accordingly, we also analyzed phase preferences of non-cue responsive neurons, including cells with multiple or diffuse spatial firing fields and cells with no obvious spatial correlate. Again, distal cells were more theta modulated than proximal cells (Rayleigh r , distal = 0.168 ± 0.006 , proximal = 0.122 ± 0.008 ; $T_{139} = 4.48$, $P < 0.0001$), and distal cells fired at a considerably earlier theta phase than proximal



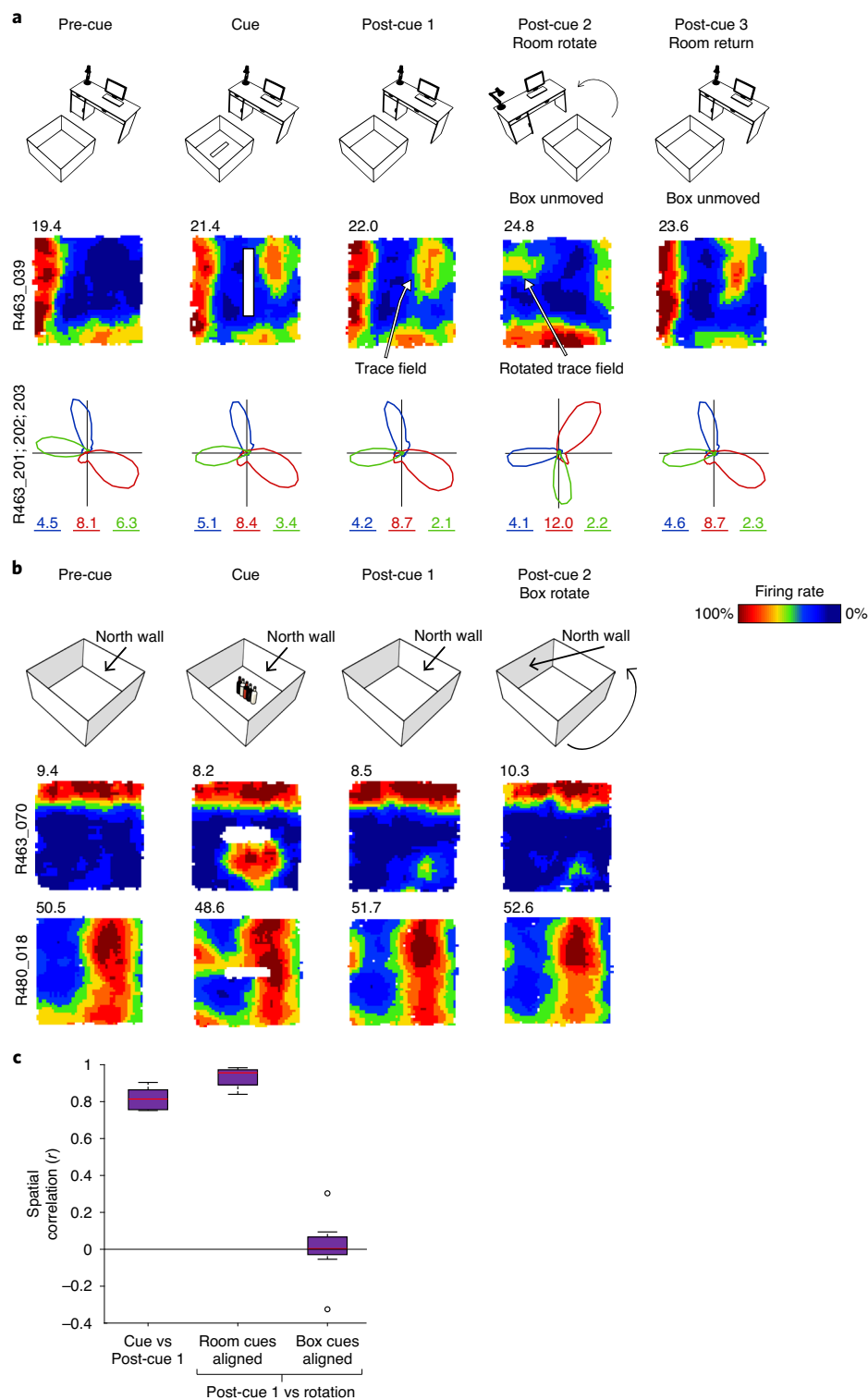


Fig. 3 | Rotation of room cues and intra-box cues show that trace fields do not reflect responses to local odor cues. **a**, Room-cues rotation manipulation (room cues rotated 90° anticlockwise; box and floor unchanged). Top: schematic of the experiment. Middle: rate maps for representative VTCs. Bottom: polar firing rate plots showing the directional tuning of three co-recorded head direction (HD) cells (marked in different colors; numbers below the polar plots show peak rate). HD cells rotated with VTC cells. **b**, Intra-box-cues rotation manipulation. Two example VTCs showing how rotating the walls and floor of the box had no effect on the location of VTC trace fields. Top: the sequence of four successive trials with two post-cue trials. For post-cue trial 2, the box and floor configuration was rotated 90° anticlockwise. Middle (rat 463) and bottom (rat 480): representative VTCs showing that the wall fields and trace fields were unaltered by the box and floor rotation. **c**, Box plots showing inter-trial correlations for VTCs ($n=13$) subjected to rotation trials, following post hoc counter rotation of rate maps to align to either room or box-and-floor cues. Boxes show 25th to 75th percentiles of each data group, the central line shows the median, and the whiskers show the extent of data 1.5× the inter-quartile range beyond the 25th and 75th percentiles. Data beyond the whisker extent are shown as individual data points. Post-cue firing fields align with room cues not box cues. Thus, fields do not reflect responses to lingering box odors.

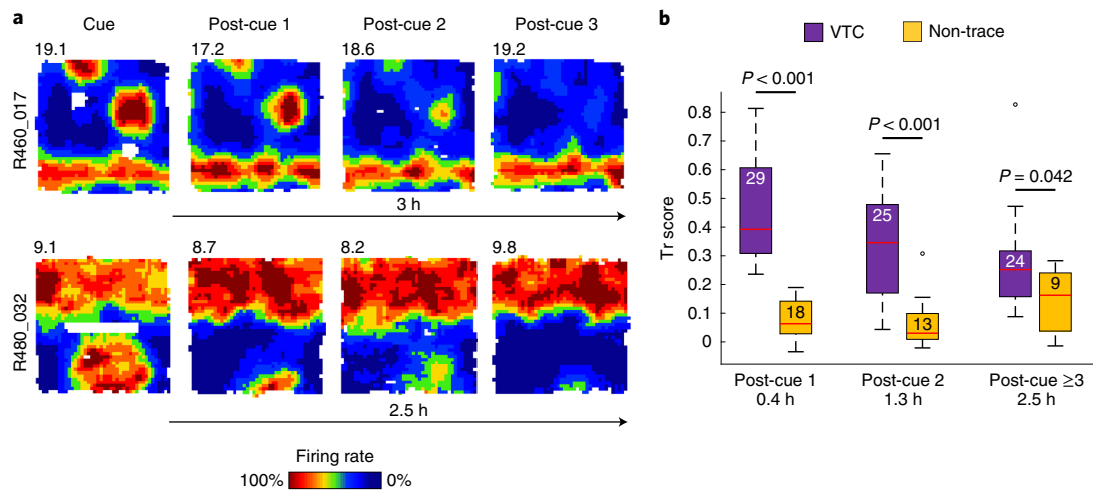


Fig. 4 | Hours-long persistence of trace fields in VTCs after cue removal. **a**, Two representative VTCs showing hours-long persistence of trace fields in the absence of cues. **b**, Box plots showing trace scores for all VTCs and non-trace cells recorded during multiple post-cue trials. Numbers within boxes indicate the number of cells sampled for each respective delay. Boxes show the 25th to 75th percentiles of each data group, the central line shows the median, and the whiskers show the extent of data 1.5× the inter-quartile range beyond the 25th and 75th percentiles. Data beyond the whisker extent are shown as individual data points. VTC trace scores decay over time, but remain significantly above non-trace cell trace scores at all time points (two tailed P values: VTC > non-trace cell simple main effect comparisons; see main text for full ANOVA details).

cells (Extended Data Fig. 5c,d): 53.2° ; distal = $163 \pm 3^\circ$, proximal = $216 \pm 10^\circ$; Watson-Williams $F_{1,139} = 40.11$, $P = 3.1 \times 10^{-9}$.

While the higher degree of theta modulation in the distal division has previously been reported²⁶, an earlier phase preference in the distal than proximal division is a novel observation. The difference in phase preference is considerable ($50\text{--}60^\circ$). Taken together, the different theta modulation and phase preference seen over various cell types strongly suggests a general principle of differing temporal organization in the proximal and distal divisions of the subiculum.

Theta phase indexed mismatch detection: preferred theta phase shifts in response to a novel cue but remains consistent in response to the familiar wall. Given the proximodistal theta differences, and the large majority of VTCs (69 out of 72) being found in the distal subiculum, we focused on the distal subiculum to investigate specifically memory-related theta modulation of VTCs. Encoding-versus-retrieval scheduling models^{4,28,29} predict that these memory-processing states are separated neurally by the theta phase of spiking, with the phase linked to the direction (potentiation and depression) and the strength of synaptic plasticity. Overall theta modulation of firing was similar for both VTCs and non-trace cells (Rayleigh r , pre-cue trial, VTCs = 0.155 ± 0.008 , non-trace = 0.166 ± 0.007 ; $T_{180} = 0.93$, $P = 0.35$). Consistent with theta scheduling models, cue insertion elicited a markedly different (earlier) preferred phase of theta in the newly generated cue field in all cue-responsive cells (Fig. 6a, top row, and see Extended Data Fig. 6 for distributions and statistics). Phase in the cue field (encoding) was earlier than in the same area in the pre-cue trial (baseline) and post-cue trial (retrieval) (-35.4° , -35.9° ; non-trace cells: -21.7° , -22.5° ; all $P < 1.8 \times 10^{-5}$). Importantly, preferred theta phase in wall fields remained constant throughout the trial sequence (Fig. 6a, bottom row, and Extended Data Fig. 7), ruling out the possibility that the cue-field earlier phase is driven by an altered global state. Thus, earlier phase indexes ‘mismatch’ detection¹⁴ and occurs in different box locations in a neuron-specific manner.

Cue-field earlier-going theta-phase change is greater in VTCs than non-trace cells. Models of hippocampal memory operations

have long posited that the hippocampus detects mismatches and that mismatch drives encoding, for example^{1,4,28,31}. Could theta phase in the cue field determine whether cue-responsive cells form a memory trace or not? There was no significant difference between the absolute phase of VTCs and non-trace cells in the cue field (Extended Data Fig. 6). However, we also tested whether the amount of within-cell late-to-early phase change following the insertion of a cue was associated with forming a memory trace. We found that VTCs showed larger phase changes in the cue field than non-trace cells when comparing cue trial (encoding) to pre-cue trial (baseline) (summary shown in Fig. 6b, left, and see Extended Data Fig. 8a for details): VTCs = $34.3 \pm 3.9^\circ$, non-trace = $21.4 \pm 3.5^\circ$; Watson-Williams $F_{1,146} = 5.72$, $P = 0.018$. A similar result was also obtained when comparing cue trial (encoding) to post-cue trial (retrieval) (Fig. 6b, right, and Extended Data Fig. 8c): VTCs = $35.1 \pm 3.4^\circ$, non-trace = $24.1 \pm 3.7^\circ$; Watson-Williams $F_{1,157} = 4.29$, $P = 0.04$. In contrast, pre-cue-cue trial and post-cue-cue trial differences in the wall field were similarly concentrated near zero for VTCs and non-trace cells (summary shown in Fig. 6b, bottom, and see Extended Data Fig. 8b,d for details): precue-cue: VTCs = $0.2 \pm 2.0^\circ$, non-trace = $359.1 \pm 1.8^\circ$; Watson-Williams $F_{1,174} = 0.17$, $P = 0.68$; postcue-cue: VTCs = $1.2 \pm 2.1^\circ$, non-trace = $0.9 \pm 1.9^\circ$; Watson-Williams $F_{1,178} = 0.01$, $P = 0.92$. The earlier theta phase in the cue field alongside the constancy of theta phase in the wall field rules out that the cue-field earlier phase is driven by an altered global state.

Figure 6c shows examples of representative individual cells, whereby preferred theta phase in the cue field is stable across pre-cue and post-cue trials, but earlier in the cue trial and earlier in VTCs than non-trace cells.

We emphasize that the changes in theta phase predicted by encoding-versus-retrieval models^{4,28} observed here do not occur in a particular region of space that is consistent for all cells, as in, for example, the choice arm (versus a side arm) of an alternation maze²⁹. Rather, cue and trace fields were distributed over the entire environment; indeed, these cue-related fields for one cell will therefore sometimes occur in the same region as the wall field of another cell (Extended Data Fig. 9). Furthermore, these cell-type-specific theta-phase changes were not driven by changes in firing rates (Extended Data Fig. 10).

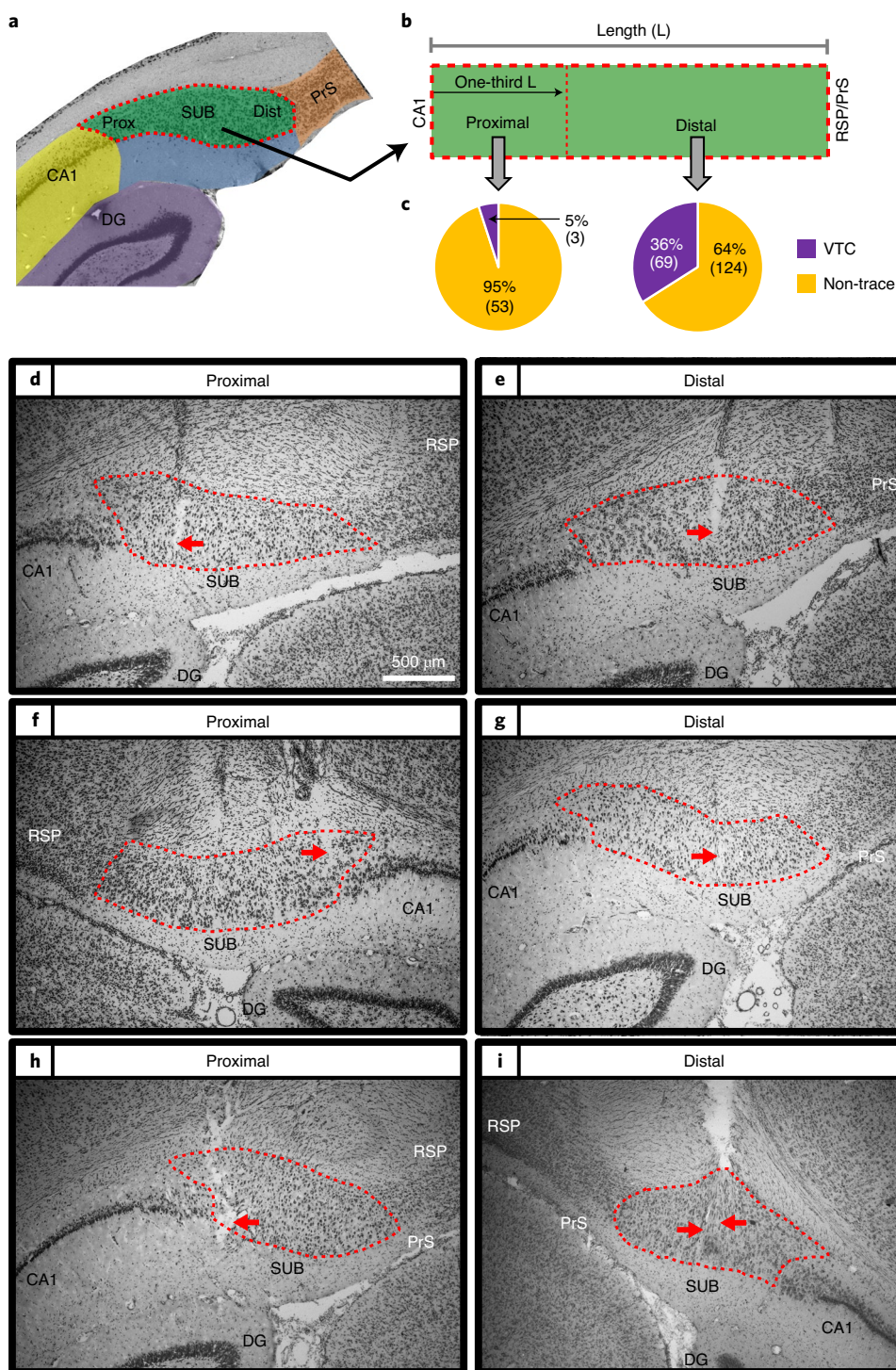


Fig. 5 | VTCs were common in the distal subiculum, but rare in the proximal subiculum. **a,b**, Recording sites were assigned to the proximal subiculum (Prox SUB; the third nearest CA1) or to the distal subiculum (Dist SUB; the two-thirds furthest from CA1) (**a**), with divisions corresponding to previously reported connectivity and gene expression patterns (**b**) (Methods). **c**, A high proportion of VTCs are present in the distal, but not the proximal, subiculum. **d–i**, Photomicrographs of coronal sections depicting representative recording sites in proximal (**d, f** and **h**) and distal (**e, g** and **i**) regions. Red arrows point to the estimated final location of the recording tetrodes. Dashed red lines indicate borders of the pyramidal layer of the subiculum. Scale bar in **d** also applies to **e–i**. Rat: 480 (**d** and **e**); 495 (**f** and **g**); 496 (**h**); 463 (**i**). DG, dentate gyrus; PrS, dorsal presubiculum; RSP, retrosplenial cortex.

Discussion

In summary, our results identify a new category of neuron, the VTC, defined by two properties. First, a VTC responds when the rat is at a specific distance and allocentric direction from a small or extended cue, including environmental boundaries, by immediately

generating a vector field. Second, the vector field persists after the cue that elicited it is subsequently removed, creating a vector trace field.

Our findings build on an emerging picture of the prevalence of vector coding in the hippocampal formation, but add the

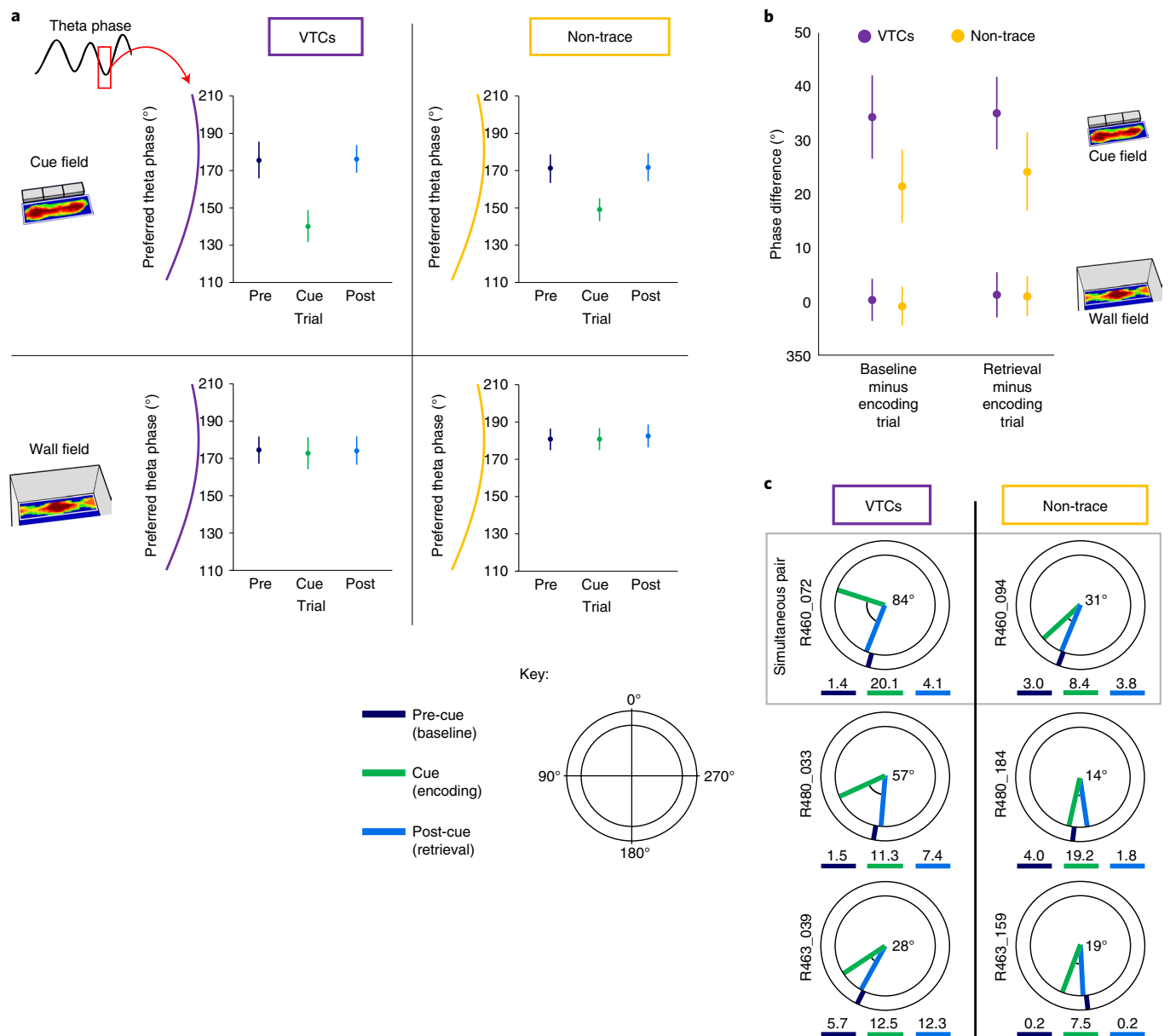


Fig. 6 | Earlier-going theta phase shift in encoding is greater in VTCs than in non-trace cells. a, Mean ($\pm 95\%$ confidence interval) preferred theta phase values for neuronal firing for the cue field (top row) and wall field (bottom row) areas. The preferred phase is markedly earlier in the cue field in the encoding trial for both VTCs (left) and non-trace cells (right) (Watson-Williams (WW) F -test: all cue-versus-pre-cue and cue-versus-post-cue $P < 1.8 \times 10^{-5}$; see Extended Data Fig. 6), but is stable for wall fields in all trials (all trial comparisons $P > 0.77$; see Extended Data Fig. 7). No adjustments were made for multiple comparisons. **b**, Mean ($\pm 95\%$ confidence interval) within-cell change in the preferred phase in the cue field area between baseline and encoding (left bars) and encoding and retrieval (right bars) for VTCs and non-trace cells. An earlier-going phase shift in the cue field, specifically in the encoding trial, is greater in VTCs (baseline minus encoding, WW F -test, $P = 0.018$; retrieval minus encoding, WW F -test, $P = 0.04$); in the wall-field, the phase difference was highly similar across cell types and concentrated near zero (WW F -test, $P \geq 0.68$). See Extended Data Fig. 7 for further details. **c**, Examples of preferred phase in the cue field area in single neurons (top VTC and non-trace co-recorded pair) from three rats, with a larger earlier-going shift in VTCs (angle shown in black at plot centers). Radial colored ticks show the mean preferred phase in each trial (see key for colors), numbers below phase diagrams show mean firing rate (Hz) in each trial.

crucial dimension of vector memory. Thus, neurons in the medial¹² and lateral³² entorhinal cortex can encode allocentric vectors to discrete objects (although not environmental boundaries), but do not show memory for previously present cues. Likewise, recent reports of egocentric vector coding of environmental cues^{33–35} also do not describe memory traces. Lateral entorhinal neurons³⁶, and a few CA1 place cells^{1,13}, can encode a memory trace for previ-

ously present objects, but these non-vectorial object fields, which develop only after cue removal, are confined to the exact object locations so cannot retrieve locations in the space between objects and boundaries as is the case for VTCs. One study³⁷ found 12% of CA1 bat cells showed egocentric vector tuning to a goal, some with memory responses. Interestingly, however, these goal-directed CA1 cells appear to encode the vector to only a single goal at a time.

The present study is the first to report a cell class that combines encoding the location of multiple cues using allocentric vectors with memory of those cue locations when the cues are removed. Importantly, the subicular representation served by VTCs seems markedly different to that in the medial entorhinal cortex, where the cells coding for vectors to objects are largely distinct from those coding for nearby environmental boundaries¹². In contrast, subicular VTCs appear to embody a global integrated representation of the entire environment, incorporating its boundaries, its objects and the relationships between all these. Overall, VTCs suggest a vector-based model of computing spatial relationships between an agent and multiple cues (or between different cues), freed from the constraints of direct perception of those cues, thus enabling spatial planning and imaginative cognition^{6–8}.

The duration of VTC memory traces in our study is in the order of 3 h. A previous study of lateral entorhinal neurons³⁶ reported much longer memory traces (several days) for a familiar object in a familiar object location, but only following extensive pretraining (typically 20 or more training sessions) to this standard object–location configuration. Indeed, in experimental conditions more similar to our own, lateral entorhinal neuron memory traces for the familiar object at novel locations, and for novel objects at novel locations, had disappeared by 3–4 h³⁶. Future work should investigate how cue exposure conditions affect the duration of VTC memory traces and whether memory trace duration is related to successful memory recall at the behavioral level.

The relative abundance and scarcity of VTCs in the distal and proximal subiculum, respectively, provide clear *in vivo* electrophysiological evidence for hypothesized spatial memory specialization along the CA1–subiculum proximal–distal pathway^{5,18,19,23}, and provide a cellular substrate for the demonstration that selective inactivation of the distal subiculum disrupts spatial memory¹⁸. This strong functional difference dovetails with our novel findings of remarkably different theta-phase preference in the distal and proximal divisions of the subiculum. That is, when referenced to the same theta local-field potential (LFP) signal, both cue-responsive cells and other cells in the distal subiculum fired 50–60° earlier than their proximal counterparts. This seemingly parallel temporal organization in the subiculum is consistent with anatomical and physiological evidence of differential pathways along the hippocampal transverse axis^{17–19,26}. The distal subiculum and the proximal CA1 (and likely the distal CA3) form one stream preferentially linked to the anterior thalamus, the medial entorhinal and the presubicular and parahippocampal cortices, while the proximal subiculum and the distal CA1 (and likely the proximal CA3) form another linked to the amygdala, the lateral entorhinal and the perirhinal and piriform cortices^{3,18,19,23,38,39}. Taken together, our findings suggest pronounced functional and temporal organizational differences between the distal and proximal divisions in the subiculum.

Finally, we note that consistent with encoding-versus-retrieval scheduling and dual-input control models of theta^{4,28,29}, all cue-responsive neurons encoded the presence of an inserted cue using an earlier phase of theta. The shift to the earlier phase was specific to the cue field, and therefore not driven by global state changes or, given the range of vectors especially in VTCs, restricted to a region in space. Rather, theta phase appeared to define a specific information channel for the presence of a newly inserted cue within each neuron. Furthermore, the degree of relative late-to-early shift, within each neuron, was linked to whether a trace field would be formed. Thus, our findings extend theta-scheduling models^{4,28,29} by demonstrating theta-phase shift as a neural substrate for memory encoding. It will be important to determine the VTC-specific factors, such as particular anatomical inputs and/or enhanced plasticity, underlying the theta-linked propensity of VTCs to generate trace fields.

An important question is whether VTCs represent a novel class of neuron, characterized by their intrinsic property of exhibiting vector trace memory in many circumstances, or whether, instead, VTCs reflect a novel type of neuronal response, which could potentially be exhibited by most subicular neurons given the appropriate experimental context. Deshmukh and Kneirim¹³ argue in this vein that, for example, time cells⁴⁰ and splitter cells⁴¹ in the CA1 are better viewed as types of responses of CA1 pyramidal cells rather than distinct types of neurons. Although we cannot currently give a definitive answer to this question, three lines of evidence argue for the former possibility that VTCs represent a class of neuron. First, VTCs exhibit specific spatial firing, anatomical and physiological features (namely, longer vector distance tunings, concentration in the distal subiculum and larger theta-phase changes in response to cues, respectively) that could not have been predicted on the basis of the original classification criteria. In our view, this increases the likelihood that VTCs describe a specific category of neuron rather than a type of neuronal response. Second, RNA sequencing and tract-tracing studies indicate that the subiculum does contain discrete categories of cell (in contrast to the CA1, which does not contain such discrete categories)^{42–44}, thereby raising the possibility that VTCs represent the functional counterpart of one or more of these anatomical/genetic categories. Third, non-trace cells exhibited a significant tendency to not produce trace responses across multiple cue types, which suggests that the lack of a trace response may be an intrinsic cell property (Extended Data Fig. 2a,b). However, we can currently only present anecdotal evidence to suggest that VTCs intrinsically form memory traces for multiple cue types (Extended Data Fig. 2c,d); further specific experiments are needed to definitively answer this question. Furthermore, we also note that residual elevated firing is present even in the cue field of non-trace cells (Extended Data Fig. 10). This may be due to imperfect classification or may suggest lower levels of memory response across a broader range of subiculum neurons. Overall, further experiments are required to definitively conclude that VTCs represent a class of neuron, and, if so, how this functional class maps onto anatomically/genetically defined categories of subiculum neurons.

Intriguingly, the distance tunings of the vectors were typically longer for trace vectors in the post-cue trial than perceptual vectors in the cue-present trial. In other words, a given vector trace field (memory recall) implies the cue was located further away than its earlier real location (during perception/encoding). This finding is reminiscent of two findings from human navigation research: (1) short navigational distances are often overestimated in memory^{45,46}, and (2) distances to viewed objects-in-context are routinely overestimated when remembered, with this bias being hippocampus-dependent⁴⁷. We speculate that the lengthening of VTC distance tunings when recalling objects may be a neural substrate for these psychological phenomena.

We have shown a code for vector memory in the subiculum for vectors in two-dimensional (2D) physical space. It seems increasingly likely that the hippocampal formation can use 2D vector-based codes of a more abstract nature to serve cognition beyond navigation^{6–9,48}. For example, grid cells can support vector calculations for navigation⁴⁹ and are able to encode a space defined by continuous abstract variables such as object features⁸, which implies that vector representations may be used to organize conceptual or semantic memories into quasi-physical spaces. Consistent with this, for instance, hippocampal activity during virtual social interactions varies with social distance defined by a vector in an abstract space involving a social power dimension and a social affiliation dimension⁵⁰. In summary, we suggest that given the flexible responsiveness of VTCs to diverse cues both within and at bounding perimeters, subicular VTCs constitute a powerful universal code for long-term vector memory in the hippocampal formation, which is of utility in spatial and non-spatial cognition.

Online content

Any methods, additional references, Nature Research reporting summaries, source data, extended data, supplementary information, acknowledgements, peer review information; details of author contributions and competing interests; and statements of data and code availability are available at <https://doi.org/10.1038/s41593-020-00761-w>.

Received: 14 October 2019; Accepted: 16 November 2020;

Published online: 21 December 2020

References

- O'Keefe, J. Place units in hippocampus of freely moving rat. *Exp. Neurol.* **51**, 78–109 (1976).
- Taube, J. S., Muller, R. U. & Ranck, J. B. Jr. Head-direction cells recorded from the postsubiculum in freely moving rats. I. Description and quantitative analysis. *J. Neurosci.* **10**, 420–435 (1990).
- Hafting, T., Fyhn, M., Molden, S., Moser, M. B. & Moser, E. I. Microstructure of a spatial map in the entorhinal cortex. *Nature* **436**, 801–806 (2005).
- Hasselmo, M. E. *How We Remember: Brain Mechanisms of Episodic Memory* (MIT Press, 2012).
- Pouster, S., Hartley, T. & Lever, C. The neurobiology of mammalian navigation. *Curr. Biol.* **28**, R1023–R1042 (2018).
- Epstein, R. A., Patai, E. Z., Julian, J. B. & Spiers, H. J. The cognitive map in humans: spatial navigation and beyond. *Nat. Neurosci.* **20**, 1504–1513 (2017).
- Bicanski, A. & Burgess, N. A neural-level model of spatial memory and imagery. *eLife* **7**, e33752 (2018).
- Constantinescu, A. O., O'Reilly, J. X. & Behrens, T. E. J. Organizing conceptual knowledge in humans with a gridlike code. *Science* **352**, 1464–1468 (2016).
- Bellmund, J. L. S., Gärdenfors, P., Moser, E. I. & Doeller, C. F. Navigating cognition: spatial codes for human thinking. *Science* **362**, eaat6766 (2018).
- Hartley, T., Burgess, N., Lever, C., Cacucci, F. & O'Keefe, J. Modeling place fields in terms of the cortical inputs to the hippocampus. *Hippocampus* **10**, 369–379 (2000).
- Lever, C., Burton, S., Jeewajee, A., O'Keefe, J. & Burgess, N. Boundary vector cells in the subiculum of the hippocampal formation. *J. Neurosci.* **29**, 9771–9777 (2009).
- Hoydal, O. A., Skytøen, E. R., Andersson, S. O., Moser, M. B. & Moser, E. I. Object-vector coding in the medial entorhinal cortex. *Nature* **568**, 400–404 (2019).
- Deshmukh, S. S. & Knierim, J. J. Influence of local objects on hippocampal representations: landmark vectors and memory. *Hippocampus* **23**, 253–267 (2013).
- Bicanski, A. & Burgess, N. Neuronal vector coding in spatial cognition. *Nat. Rev. Neurosci.* **21**, 453–470 (2020).
- Gallistel, C. R. *The Organization of Learning* (MIT Press, 1990).
- Poucet, B. Spatial cognitive maps in animals: new hypotheses on their structure and neural mechanisms. *Psychol. Rev.* **100**, 163–182 (1993).
- Witter, M. P. & Groenewegen, H. J. The subiculum: cytoarchitecturally a simple structure, but hodologically complex. *Prog. Brain Res.* **83**, 47–58 (1990).
- Cembrowski, M. S. et al. Dissociable structural and functional hippocampal outputs via distinct subiculum cell classes. *Cell* **173**, 1280–1292.e18 (2018).
- Bienkowski, M. S. et al. Integration of gene expression and brain-wide connectivity reveals the multiscale organization of mouse hippocampal networks. *Nat. Neurosci.* **21**, 1628–1643 (2018).
- Roy, D. S. et al. Distinct neural circuits for the formation and retrieval of episodic memories. *Cell* **170**, 1000–1012.e19 (2017).
- Nitzan, N. et al. Propagation of hippocampal ripples to the neocortex by way of a subiculum–retrosplenial pathway. *Nat. Commun.* **11**, 1947 (2020).
- Braga, R. M., Van Dijk, K. R. A., Polimeni, J. R., Eldaief, M. C. & Buckner, R. L. Parallel distributed networks resolved at high resolution reveal close juxtaposition of distinct regions. *J. Neurophysiol.* **121**, 1513–1534 (2019).
- Knierim, J. J., Neunuebel, J. P. & Deshmukh, S. S. Functional correlates of the lateral and medial entorhinal cortex: objects, path integration and local-global reference frames. *Philos. Trans. R. Soc. Lond. B Biol. Sci.* **369**, 20130369 (2014).
- Olson, J. M., Tongprasearth, K. & Nitz, D. A. Subiculum neurons map the current axis of travel. *Nat. Neurosci.* **20**, 170–172 (2017).
- Sharp, P. E. & Green, C. Spatial correlates of firing patterns of single cells in the subiculum of the freely moving rat. *J. Neurosci.* **14**, 2339–2356 (1994).
- Kim, S. M., Ganguli, S. & Frank, L. M. Spatial information outflow from the hippocampal circuit: distributed spatial coding and phase precession in the subiculum. *J. Neurosci.* **32**, 11539–11558 (2012).
- Giocomo, L. M. et al. Topography of head direction cells in medial entorhinal cortex. *Curr. Biol.* **24**, 252–262 (2014).
- Hasselmo, M. E., Bodelon, C. & Wyble, B. P. A proposed function for hippocampal theta rhythm: separate phases of encoding and retrieval enhance reversal of prior learning. *Neural Comput.* **14**, 793–817 (2002).
- Fernandez-Ruiz, A. et al. Entorhinal–CA3 dual-input control of spike timing in the hippocampus by theta–gamma coupling. *Neuron* **93**, 1213–1226.e5 (2017).
- Douchamps, V., Jeewajee, A., Blundell, P., Burgess, N. & Lever, C. Evidence for encoding versus retrieval scheduling in the hippocampus by theta phase and acetylcholine. *J. Neurosci.* **33**, 8689–8704 (2013).
- Hasselmo, M. E. & Schnell, E. Laminar selectivity of the cholinergic suppression of synaptic transmission in rat hippocampal region CA1: computational modeling and brain slice physiology. *J. Neurosci.* **14**, 3898–3914 (1994).
- Deshmukh, S. S. & Knierim, J. J. Representation of non-spatial and spatial information in the lateral entorhinal cortex. *Front. Behav. Neurosci.* **5**, 69 (2011).
- Wang, C. et al. Egocentric coding of external items in the lateral entorhinal cortex. *Science* **362**, 945–949 (2018).
- Hinman, J. R., Chapman, G. W. & Hasselmo, M. E. Neuronal representation of environmental boundaries in egocentric coordinates. *Nat. Commun.* **10**, 2772 (2019).
- Alexander, A. S. et al. Egocentric boundary vector tuning of the retrosplenial cortex. *Sci. Adv.* **6**, eaaz2322 (2020).
- Tsao, A., Moser, M. B. & Moser, E. I. Traces of experience in the lateral entorhinal cortex. *Curr. Biol.* **23**, 399–405 (2013).
- Sarel, A., Finkelstein, A., Las, L. & Ulanovsky, N. Vectorial representation of spatial goals in the hippocampus of bats. *Science* **355**, 176–180 (2017).
- Henriksen, E. J. et al. Spatial representation along the proximodistal axis of CA1. *Neuron* **68**, 127–137 (2010).
- Lee, H., Wang, C., Deshmukh, S. S. & Knierim, J. J. Neural population evidence of functional heterogeneity along the CA3 transverse axis: pattern completion versus pattern separation. *Neuron* **87**, 1093–1105 (2015).
- MacDonald, C. J., Lepage, K. Q., Eden, U. T. & Eichenbaum, H. Hippocampal “time cells” bridge the gap in memory for discontinuous events. *Neuron* **71**, 737–749 (2011).
- Wood, E. R., Dudchenko, P. A., Robitsek, R. J. & Eichenbaum, H. Hippocampal neurons encode information about different types of memory episodes occurring in the same location. *Neuron* **27**, 623–633 (2000).
- Cembrowski, M. S. et al. The subiculum is a patchwork of discrete subregions. *eLife* **7**, e37701 (2018).
- Ding, S.-L. et al. Distinct transcriptomic cell types and neural circuits of the subiculum and prosubiculum along the dorsal–ventral axis. *Cell Rep.* **31**, 107648 (2020).
- Cembrowski, M. S. et al. Spatial gene-expression gradients underlie prominent heterogeneity of CA1 pyramidal neurons. *Neuron* **89**, 351–368 (2016).
- Lederman, S. J., Klatzky, R. L., Collins, A. & Wardell, J. Exploring environments by hand or foot: time-based heuristics for encoding distance in movement space. *J. Exp. Psychol. Learn. Mem. Cogn.* **13**, 606–614 (1987).
- Lloyd, R. & Heivly, C. Systematic distortions in urban cognitive maps. *Ann. Assoc. Am. Geogr.* **77**, 191–207 (1987).
- Mullally, S. L., Intraub, H. & Maguire, E. A. Attenuated boundary extension produces a paradoxical memory advantage in amnesic patients. *Curr. Biol.* **22**, 261–268 (2012).
- O'Keefe, J. in *Representing Direction in Language and Space* (eds van der Zee, E. & Slack, J.) Ch. 4 (Oxford Univ. Press, 2003).
- Bush, D., Barry, C., Manson, D. & Burgess, N. Using grid cells for navigation. *Neuron* **87**, 507–520 (2015).
- Tavares, R. M. et al. A map for social navigation in the human brain. *Neuron* **87**, 231–243 (2015).

Publisher's note Springer Nature remains neutral with regard to jurisdictional claims in published maps and institutional affiliations.

© The Author(s), under exclusive licence to Springer Nature America, Inc. 2020

Methods

Subjects. Six male Lister hooded rats, weighing 392–522 g (aged 3–5 months) at the time of surgery, were used as subjects. All rats were maintained on a 12–12-h light–dark schedule (with lights off at 10:00; all animals were tested during their dark phase). Food deprivation (after rats had recovered from surgery) was maintained during recording periods such that subjects weighed 85–90% of free feeding weight. All experiments were performed under the Animals (Scientific Procedures) Act 1986. Approval for the animal experiments was granted by both Durham University AWERB and the UK Home Office Project and Personal Licenses.

Surgery and tetrode implants. Under deep anesthesia (1–3% isoflurane) and using intra- and post-operative analgesia (buprenorphine, 0.04 mg per kg), rats were chronically implanted with two microdrives (one above the dorsal subiculum of each hemisphere). These microdrives allowed four or eight tetrodes to be vertically lowered through the brain. The eight-tetrode-loaded microdrives (implanted in four rats) used custom three-dimensionally-printed barrels to create a 4×2 tetrode array (150- μ m spacing between barrel holes). With the four-tetrode-loaded microdrives (implanted in two rats), all the tetrodes were loaded using a single cannula. Tetrodes were constructed from HM-L-coated platinum–iridium wire (90%/10%, California Fine Wire, 25 μ m). The details of tetrode mapping for each drive were recorded using photographs and notes both before surgery and after perfusion.

Subiculum: implant co-ordinates and histology. Our implants targeted the anterior portion of the dorsal subiculum. The skull coordinates used for insertion of the centroid of the tetrode array were based on ref.⁵¹ in the following range: anterior–posterior (AP): –5.8 to –6.4 mm; medial–lateral (ML): \pm 2.9–3.3 mm. Details of recording sites were reconstructed using records of electrode movement, physiological markers and post-mortem histology. The rats were killed and transcardially perfused with saline followed by 4% paraformaldehyde. Each brain was coronally sliced into 40- μ m thick sections, mounted and Nissl-stained (using cresyl violet or thionin) for visualization of the electrode tracks/tips. Digital photomicrographs were converted from color to black and white, and contrast and brightness adjusted, using Photoshop Express 3.5. Data from recording sites in the CA1 or the dorsal presubiculum were excluded, and recording sites in the subiculum were classified as being located in either the proximal subiculum or the distal subiculum (see next section). Representative recording locations are shown in Fig. 5.

Parcellating the subiculum into proximal and distal zones. The proximodistal axis has long been thought to be important in the functional anatomy of the subiculum: the distal subiculum and the proximal CA1 (and likely the distal CA3) form a stream linked to spatial memory, while the proximal subiculum and the distal CA1 (and likely the proximal CA3) form a stream linked to object memory (for examples, see refs.^{17–19,23,26,38,39,43,52–58}). In the subiculum, the proximal pole abuts the CA1, and the distal pole abuts the retrosplenial cortex/presubiculum. In the present study, the coronal sections were used to classify recording sites as belonging to either the proximal zone, consisting of the third closest to the CA1, or to the distal zone, consisting of the two-thirds furthest from the CA1. The rationale for this approach was twofold. First, the distal two-thirds of the subiculum define a region that projects heavily onto cortical regions linked to spatial memory (medial entorhinal, retrosplenial, dorsal presubicular and parasubicular cortices; for examples, see refs.^{43,57,59}). Second, the proximal subiculum (termed ‘prosubiculum’ in refs.^{19,43,60} as defined by gene and protein expression patterns) occupies approximately one-third of the proximodistal extent of the anterodorsal subiculum (see coronal sections 81–89 in supplementary figure 1 of ref.¹⁹ and see ref.⁶¹).

Electrophysiological recording. Rats were allowed 1 week to recover post-operatively before screening sessions began. During screening and inter-trial intervals, the rat rested on a square holding platform (40-cm sides, 5-cm high ridges) containing sawdust. Tetrodes were gradually lowered toward the subiculum pyramidal layer over days/weeks. Tetrodes were left to stabilize for at least 24 h after tetrode movement before recording commenced. Electrophysiological data from screening and recording sessions were obtained using Axona DACQ systems (DacqUSB). Electrode wires were AC-coupled to unity-gain buffer amplifiers (headstage). Lightweight wires (~4 m) were connected the headstage to a pre-amplifier (gain 1,000). The outputs of the pre-amplifier passed through a switching matrix, and then to the filters and amplifiers of the recording system (Axona). Signals were amplified (6,500–14,000) and band-pass filtered (500 Hz to 7 kHz). Each channel was continuously monitored at a sampling rate of 50 kHz, and action potentials were stored as 50 points per channel (1 ms, with 200- μ s pre-threshold and 800- μ s post-threshold) whenever the signal from any of the 4 channels of a tetrode exceeded a given threshold. LFP signals were amplified 3,500–5,000, band-pass filtered at 0.34–125 Hz and sampled at 250 Hz. Two arrays of infrared light-emitting diodes (LEDs), one array larger than the other for tracking discriminability, were attached to the head of the rat to track head position and orientation using a video camera and tracking hardware/software (DacqUSB,

Axona). The arrays of LEDs were positioned such that the halfway position between the two arrays was centered above the skull of the rat. Offline analysis defined this halfway position as the position of the rat (TINT, Axona). Positions were sampled at 50 Hz.

Testing laboratory and recording environments. External cues such as a lamp, PC monitor and cue cards on the walls provided directional constancy throughout the test trial series. For every trial, the rat was carried directly from the holding platform with its head facing toward the recording arena. During trials, the rat searched for grains of sweetened rice randomly thrown into the box about every 30 s. At the end of each trial, the rat was removed from the recording environment and placed back on the holding platform until the next trial. Inter-trial intervals varied from 10 min to 1 h, but were typically around 25 min. The standard recording environment was a square box (100×100×50-cm high) painted in ‘light rain’ gray. Occasionally, for more distally tuned cells, a larger, same colored environment was used (either 150×150×50-cm high or 150×190×50-cm high). Four types of cue, introduced into the box during the cue trial, were used (refer to Fig. 1 for diagrams): a black painted barrier (50×2.5×50-cm high); three wooden black bricks juxtaposed along their long axis (20×9.5×4.5-cm high), thus creating a 60×28.5×4.5-cm high cue; a high-contrast white stencil-painted stripe (60×10×0-cm high) acting as a purely visual cue; and wine bottles (base diameter 7 cm, 30-cm high) painted with different large, high-contrast patterns and/or affixed with somatosensorily different patches. In some trials, only one bottle was inserted into the environment. In other trials, two or more bottles were inserted in different configurations: tightly juxtaposed in an array to create a continuous barrier, placed apart to create a linear spaced array or placed apart in different regions of the box.

Standard test trial sequence and variants. The standard test trial sequence consisted of three consecutive trials: (1) a pre-cue trial, in which the recording box contained no cue; (2) a cue trial, in which the box contained one of the abovementioned four types of cue; and (3) a post-cue trial, in which the box again contained no cue. In a minority of sessions, one variant of the standard test sequence was that more than one cue trial was run successively before the post-cue trial. In this case, only the first cue trial was used to define the cue field and cue responsiveness of the neuron. This procedure had no significant effect on the probability of a trace response arising (successive multiple cue trials 42% trace, single cue trials of matched cue type (barrier), 33% trace; Z-test for proportions: $Z=0.84$, $P=0.40$). In other cases, the experimental session was extended to include a repeat of the standard three-trial sequence (pre-cue trial, cue trial, post-cue trial), most often with physically different cues. In these cases, only the single cue trial with the strongest cue-elicited field (that is, highest integrated firing rate, see description below) and its accompanying pre-cue and post-cue trials were selected for main analysis. Responses to the full set of cues are described in Extended Data Fig. 2.

Extended post-cue trial sequences including rotation trials. In some sessions, two or more post-cue trials were successively run. This enabled evaluation of how long trace fields persisted in the recording box in the continued absence of the cues that elicited them. In some instances, we also included a ‘rotation’ trial in this post-cue trial sequence to test for the potential influence of uncontrolled local odors on trace fields. Rotation trials took two forms: (1) the local, intra-box cues (box-and-floor ensemble) was rotated 90° anticlockwise with respect to room; and (2) external cues such as lamps and tables were rotated, while the intra-box cues maintained their orientation with respect to the testing room. As trace fields failed to rotate in all cases of type (1) rotation (Fig. 2), these trials were also included in the analysis evaluating how long trace fields persisted in the recording box and in the absence of cue objects.

Cell isolation. Cluster cutting to isolate single units was performed using a combination of KlustaKwik (v.3)⁶² and manual isolation using TINT (Axona). All the trials from a given session were loaded into TINT as a merged dataset, which was clustered using KlustaKwik’s principal component analysis. Subsequent manual adjustments were made where necessary. Once merged-trial cutting was complete, cell clusters were automatically split into each individual trial of that session (Axona MultiCutSplitter).

Firing-rate maps. Firing-rate maps for all recorded neurons were produced by first dividing the recording arena into a grid of 2×2-cm square spatial bins and finding the summed occupancy time and number of spikes fired in each bin. Summed occupancy and spiking maps were then smoothed with a 10×10-cm boxcar kernel, and rate maps were constructed by dividing summed spiking by summed occupancy. Data from periods of immobility (movement speed <5 cm s⁻¹) were excluded from rate maps, so as to restrict the analysis to neural firing from theta epochs, and exclude firing occurring during sharp-wave ripple epochs. Removal of immobility produced a very small but significant increase in the within-trial spatial stability of firing. A similar, but nonsignificant, trend was observed for firing specifically within the cue field (Supplementary Fig. 1).

Definition of cue fields and cue-responsive neurons. New firing fields generated by the insertion of a cue were detected as follows. First, firing-rate maps were converted to z -scores to allow comparison between different trials, even following trial-to-trial fluctuations in the firing rate. For each map, values for each bin had the overall mean firing rate subtracted and were then divided by the overall variance of the firing rate across bins. Following this, the z -scored pre-cue map was subtracted from the z -scored cue map, thus producing a map describing where firing was increased specifically during the cue trial relative to the pre-cue trial. Cue fields were then defined as contiguous regions of the resulting map with a value of ≥ 1 . If more than one cue field was present, only the largest was used for further analysis. Cue-responsive cells were defined as those where the sum of z -scored firing rate, within the cue field, was ≥ 70 .

Definition of trace and overlap scores. To define trace and overlap scores, cue and post-cue firing-rate maps were z -scored, and the pre-cue map was subtracted from both, so as to highlight changes in firing relative to the pre-cue trial (the same procedure as described above, “Definition of cue fields and cue-responsive neurons”). The trace score was defined as the mean value of z -scored firing within the cue field region (as defined above) in the post-cue trial, divided by the mean of z -scored firing within the cue field region in the cue trial. A trace score of 1 therefore indicates a memory-based response of equal strength to that induced by the presence of the cue. To define the overlap score, we first detected whether any new regions of firing existed in the post-cue trial, relative to the pre-cue trial: such post-cue fields were defined as contiguous regions of the (z -scored, pre-cue subtracted) post-cue map with a value of ≥ 1 . If several post-cue fields existed, only the largest was used for further analysis. If a post-cue field was present, the overlap score was defined as follows:

$$\left(\frac{\sum \text{FR}_{\text{Ov}}}{\sum \text{FR}_{\text{Post}}} + \frac{\sum \text{FR}_{\text{Ov}}}{\sum \text{FR}_{\text{Cue}}} \right) / 2$$

Where $\sum \text{FR}$ in all cases refers to the summed firing rate in a region of the post-cue trial rate map: $\sum \text{FR}_{\text{Post}}$ being the summed rate in the post-cue field, $\sum \text{FR}_{\text{Cue}}$ the summed rate in the cue field and $\sum \text{FR}_{\text{Ov}}$ being the summed rate in the overlap between the cue and post-cue fields. The overlap score therefore assesses the average extent to which post-cue field firing overlaps the cue field firing, and vice versa. Where no post-cue field was present, the overlap score was set to zero.

Spatially randomized trace and overlap scores. To calculate whether the proportion of VTCs observed in our dataset exceeded that expected by chance, we constructed a population of trace and overlap scores derived from a spatially randomized dataset. Spatial randomization was performed by first calculating the cue-field position from the cue map, as per normal analysis (see above). Then, the mask representing the region defined as the cue field was subjected to a random rotation and shift, before trace and overlap scores were calculated using post-cue map. Spatially randomized scores therefore assessed the presence of memory-based firing in a spatially random part of the post-cue trial. Spatial shifts of the cue-field mask were subject to two constraints: (1) the shifted, rotated mask must lie entirely within the recording arena, and (2) the shifted, rotated mask must not overlap with the pre-existing fields (wall fields) in the pre-cue trial (defined as contiguous areas with z -scored firing of ≥ 1). This process was repeated 1,000 times for each neuron. Finally, VTCs were then defined as cells whose trace scores were greater than the 90th percentile of the spatially randomized trace scores, and whose overlap scores were greater than the 90th percentile of the spatially randomized trace scores.

Vector spatial firing analysis. To characterize how VTCs and non-trace cells fired as a function of vector displacement from the cue, we constructed vector-displacement firing-rate maps, akin to those in ref. 12, which show the overall mean firing rate at each specific angular and distance displacement. However, the abovementioned study calculated vector displacements by approximating the position of the (small) cue object as a point in space, which was not feasible for our data, where the many cues were extended objects (for example, barriers). We therefore began by calculating the set of vector displacements to the cue object that occurred at each spatial bin (defined here as a bin in the 2D rate map): for each spatial bin, we calculated the mean distance to the cue in every angular vector bin. Only the sides of the cue object not occluded by other sides, given the spatial position under consideration, were considered. Distances for angles in which the cue was not encountered at all were set to a null value. Angular vector bins were 6° wide. Then, the vector displacement map, describing mean cell firing at displacement angles $A_1 - A_n$ and distances $D_1 - D_m$, was constructed as follows. The value of the vector map describing firing at angle = A and distance = D was defined as the mean of the firing rates of all those spatial bins where the displacement vector for angle A fell between the upper and lower limits of distance bin D . Distance bins were 2.5-cm wide. Intuitively, therefore, each bin in a vector-displacement rate map shows the mean firing rates over all those spatial bins where at least one of the displacement vectors to the cue match the specified vector angle and distance.

Following the construction of vector-displacement maps, vector tunings for each neuron were defined by first isolating contiguous areas of elevated firing in the vector map (>1 standard deviation above mean for the whole map). Following this step, the distance and angle tuning were defined as the firing rate-weighted centroid of the largest contiguous area of elevated firing. To describe the vector tuning of firing specifically linked to cue presence or cue memory, only spatial bins in the cue field (for cue tunings) and the post-cue field (for memory-trace tunings) were used to construct the vector-displacement map. Vector-displacement maps for wall fields in the pre-cue trial were constructed using the same methods as described above, with the exceptions that the vectors were calculated to the positions of the arena walls, instead of to cues, and only spatial bins in the wall field contributed to the construction of the vector map. Cells for which the cue trial consisted of multiple separated objects were excluded from the vector analysis due to the difficulty in resolving the ambiguity of which cue object the firing fields represented the vector displacement to. Due to the physical constrictions of space within the arena around some objects, not all vector displacements can be sampled: these vectors are shown as dark gray in the vector maps. Vector maps were converted to a circular display, with upsampled, interpolated bins, to enhance their clarity and comprehensibility for display purposes only: all calculations described above were applied to a binned map of 6° -angle bins and 2.5-cm distance bins.

Theta-firing-phase analysis. Instantaneous theta phase was defined by filtering LFPs using a 5–11-Hz band-pass filter and taking the angle of the Hilbert-transformed filtered signal. The theta phase of each spike was defined as the phase of the temporally corresponding LFP sample, from the hemisphere-matched LFP in the distal subiculum with the highest signal-to-noise ratio for the theta oscillation. The signal-to-noise ratio for theta was defined as the mean power in the theta band (± 0.5 Hz around the highest power between 7 and 10 Hz) divided by the mean power in the range 2–20 Hz, excluding the theta band. Spectral power was estimated using the fast-Fourier transform. The overall theta modulation of each neuron was estimated using the length of the resultant mean vector of phases. As with rate maps, speed filtering (>5 cm s^{-1} epochs passing) was applied; only neurons firing ≥ 50 spikes while the animal occupied the relevant firing field (over the course of a whole trial), and with significant theta phase modulation (defined as Rayleigh test $P < 0.01$), were used for phase analysis^{63–65}. This was done to remove the influence of noisy data. The preferred firing phase of each neuron, in each firing field, was defined as the circular mean of the spike phases for spikes occurring while the rat was within the given firing field (wall field, cue-field regions). The above steps were performed using custom-written Matlab scripts. Subsequent circular statistical analyses were conducted in Oriana 4 (see the section “Circular statistics” below).

Statistics. No statistical methods were used to predetermine sample sizes (cell numbers). All available sessions where cue-responsive cells were present and thus vector trace cells could have been observed (that is, pre-cue, cue, post-cue trial series) were analyzed. Our sample sizes were similar to sample sizes reported in previous publications^{12,24,33–37}. Cues were varied (see below) but there was no formal randomization in the organization of stimulus presentations. Data collection and analysis were not performed blind to the conditions of the experiments.

Data distribution in linear tests was assumed to be normal and with equal variance, but this was not formally tested. Welch t -tests were applied to analysis of distance vectors since these distributions across the VTC and non-trace groups were of unequal variance. All linear statistical tests were conducted as two-tailed. There are no equivalents to tail number choices in the circular statistical tests employed in this report, that is, the three tests of departure from uniformity (Rayleigh’s r , Watson’s U^2 and Kuiper’s V), and the Watson–Williams F -test.

Circular statistics: theta-phase data. After the Matlab steps described in the preceding section “Theta-phase-firing analysis”, theta-phase data was analyzed in Oriana 4 (Kovach Computing).

Distributions of neuronal preferred phases (for example, distal cells and VTCs) were characterized by the following: the mean phase, that is, the circular mean of the neuronal preferred phases; the circular standard error of the mean (in the main text); 95% confidence limits (in figures); Rayleigh vector r ; and Von Mises κ (indexing concentration). The difference between mean absolute preferred phases was tested using Watson–Williams F -tests. The shift of preferred spike phase was defined by the circular phase difference between two given trials in a given cue or wall field, with the differences then tested using Watson–Williams F -tests.

Circular statistics: angular tunings in vector-displacement maps. To test for multimodal departures from uniformity such as angular biasing by north–south and east–west oriented cue and wall placements, we first applied Rayleigh’s test of uniformity, then Watson’s U^2 and Kuiper’s V tests⁶⁶. Rayleigh’s test is much more sensitive to unimodal departures from uniformity than Watson’s U^2 and Kuiper’s V tests. When a distribution is far from departing from uniformity as indexed by Rayleigh’s unimodal test, but significantly departs from uniformity as indexed by the omnibus tests (Watson’s U^2 and Kuiper’s V), we interpret this as consistent with showing multimodal departures from uniformity.

Reproducibility. There were no separate replication experiments. Reproducibility was inferred by the observation of VTCs in the distal subiculum of each of the six rats tested, with mean per-rat proportion (35%; breakdown 17% (3 out of 17); 29% (20 out of 68); 33% (2 out of 6); 36% (15 out of 42); 47% (8 out of 17); 50% (21 out of 42)) similar to total proportion (36%; shown in Fig. 5b). Not all subicular cue-responsive cell ensembles contained VTCs. However, some ensembles contained just one or two cue-responsive cells and/or sampled only from the proximal subiculum, where (as described in the main text and Fig. 5) VTCs are rare.

Reporting Summary. Further information on research design is available in the Nature Research Reporting Summary linked to this article.

Data availability

Data are available upon reasonable request from the authors.

Code availability

Key custom Matlab code, including that for defining trace and overlap scores and constructing vector-rate maps, will be made publicly available at <https://github.com/WillsCacucciLab/VectorTraceCode>.

References

- Paxinos, G. & Watson, C. *The Rat Brain in Stereotaxic Coordinates* 6th edn (Academic Press/Elsevier, 2007).
- Tamamaki, N. & Nojyo, Y. Preservation of topography in the connections between the subiculum, field CA1, and the entorhinal cortex in rats. *J. Comp. Neurol.* **353**, 379–390 (1995).
- O'Mara, S. M., Commins, S., Anderson, M. & Gigg, J. The subiculum: a review of form, physiology and function. *Prog. Neurobiol.* **64**, 129–155 (2001).
- Kim, Y. & Spruston, N. Target-specific output patterns are predicted by the distribution of regular-spiking and bursting pyramidal neurons in the subiculum. *Hippocampus* **22**, 693–706 (2012).
- Sun, Y. et al. Cell-type-specific circuit connectivity of hippocampal CA1 revealed through Cre-dependent rabies tracing. *Cell Rep.* **7**, 269–280 (2014).
- Aggleton, J. P. & Christiansen, K. The subiculum: the heart of the extended hippocampal system. *Prog. Brain Res.* **219**, 65–82 (2015).
- O'Reilly, K. C., Gulden Dahl, A., Ulsaker Kruge, I. & Witter, M. P. Subicular-parahippocampal projections revisited: development of a complex topography in the rat. *J. Comp. Neurol.* **521**, 4284–4299 (2013).
- Nakamura, N. H., Flasbeck, V., Maingret, N., Kitsukawa, T. & Sauvage, M. M. Proximodistal segregation of nonspatial information in CA3: preferential recruitment of a proximal CA3–distal CA1 network in nonspatial recognition memory. *J. Neurosci.* **33**, 11506–11514 (2013).
- Ishihara, Y. & Fukuda, T. Immunohistochemical investigation of the internal structure of the mouse subiculum. *Neuroscience* **337**, 242–266 (2016).
- Ding, S. L. Comparative anatomy of the prosubiculum, subiculum, presubiculum, postsubiculum, and parasubiculum in human, monkey, and rodent. *J. Comp. Neurol.* **521**, 4145–4162 (2013).
- Slomianka, L. & Geneser, F. A. Distribution of acetylcholinesterase in the hippocampal region of the mouse: II. Subiculum and hippocampus. *J. Comp. Neurol.* **312**, 525–536 (1991).
- Kadir, S. N., Goodman, D. F. M. & Harris, K. D. High-dimensional cluster analysis with the masked EM algorithm. *Neural Comput.* **26**, 2379–2394 (2014).
- Jones, M. W. & Wilson, M. A. Theta rhythms coordinate hippocampal–prefrontal interactions in a spatial memory task. *PLoS Biol.* **3**, e402 (2005).
- Mizuseki, K., Sirota, A., Pastalkova, E. & Buzsáki, G. Theta oscillations provide temporal windows for local circuit computation in the entorhinal–hippocampal loop. *Neuron* **64**, 267–280 (2009).
- Mizuseki, K., Diba, K., Pastalkova, E. & Buzsáki, G. Hippocampal CA1 pyramidal cells form functionally distinct sublayers. *Nat. Neurosci.* **14**, 1174–1181 (2011).
- Pewsey, A., Neuhäuser, M. & Ruxton, G. D. *Circular Statistics in R* (Oxford Univ. Press, 2013).
- Derdikman, D. Are the boundary-related cells in the subiculum boundary-vector cells? *J. Neurosci.* **29**, 13429–13431 (2009).
- Mehta, M. R., Lee, A. K. & Wilson, M. A. Role of experience and oscillations in transforming a rate code into a temporal code. *Nature* **417**, 741–746 (2002).
- Harris, K. D. et al. Spike train dynamics predicts theta-related phase precession in hippocampal pyramidal cells. *Nature* **417**, 738–741 (2002).
- Huxter, J., Burgess, N. & O'Keefe, J. Independent rate and temporal coding in hippocampal pyramidal cells. *Nature* **425**, 828–832 (2003).

Acknowledgements

We thank E. Stanton, A. Long and S. Thurlbeck for technical assistance. We thank N. Burgess and D. Bush for helpful comments on an earlier version of this manuscript. We acknowledge funding from the BBSRC (BB/M008975/1 to C.L. and co-investigator T.J.W.; BB/T014768/1 to C.L. & co-investigator S.P.), the Royal Society (UF100746 to T.J.W.), the MRC (MR/N026012/1 to T.J.W.) and start-up funds from CIMEC, Trento, Italy (to S.A.L.).

Author contributions

S.P. and C.L. conceptualized and designed the study. S.P. performed the experiments. S.P., T.J.W. and C.L. analyzed the data and wrote the manuscript. S.A.L. contributed to conceptualization, experimental design and training. J.D. contributed to training, surgery and histology. C.L., S.P., T.J.W. and S.A.L. contributed to funding acquisition. All the authors discussed the results and contributed to the manuscript.

Competing interests

The authors declare no competing interests.

Additional information

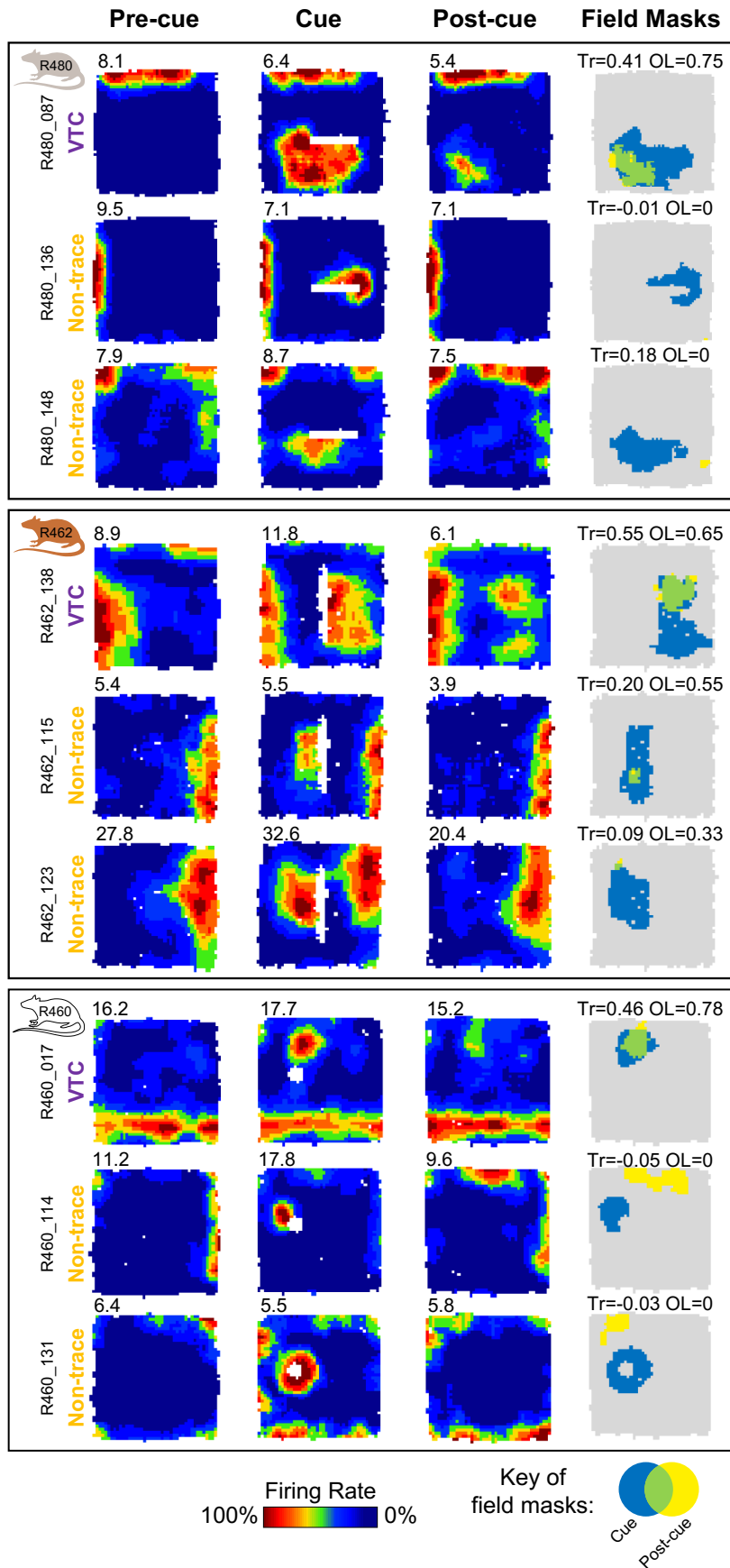
Extended data is available for this paper at <https://doi.org/10.1038/s41593-020-00761-w>.

Supplementary information is available for this paper at <https://doi.org/10.1038/s41593-020-00761-w>.

Correspondence and requests for materials should be addressed to S.P., T.J.W. or C.L.

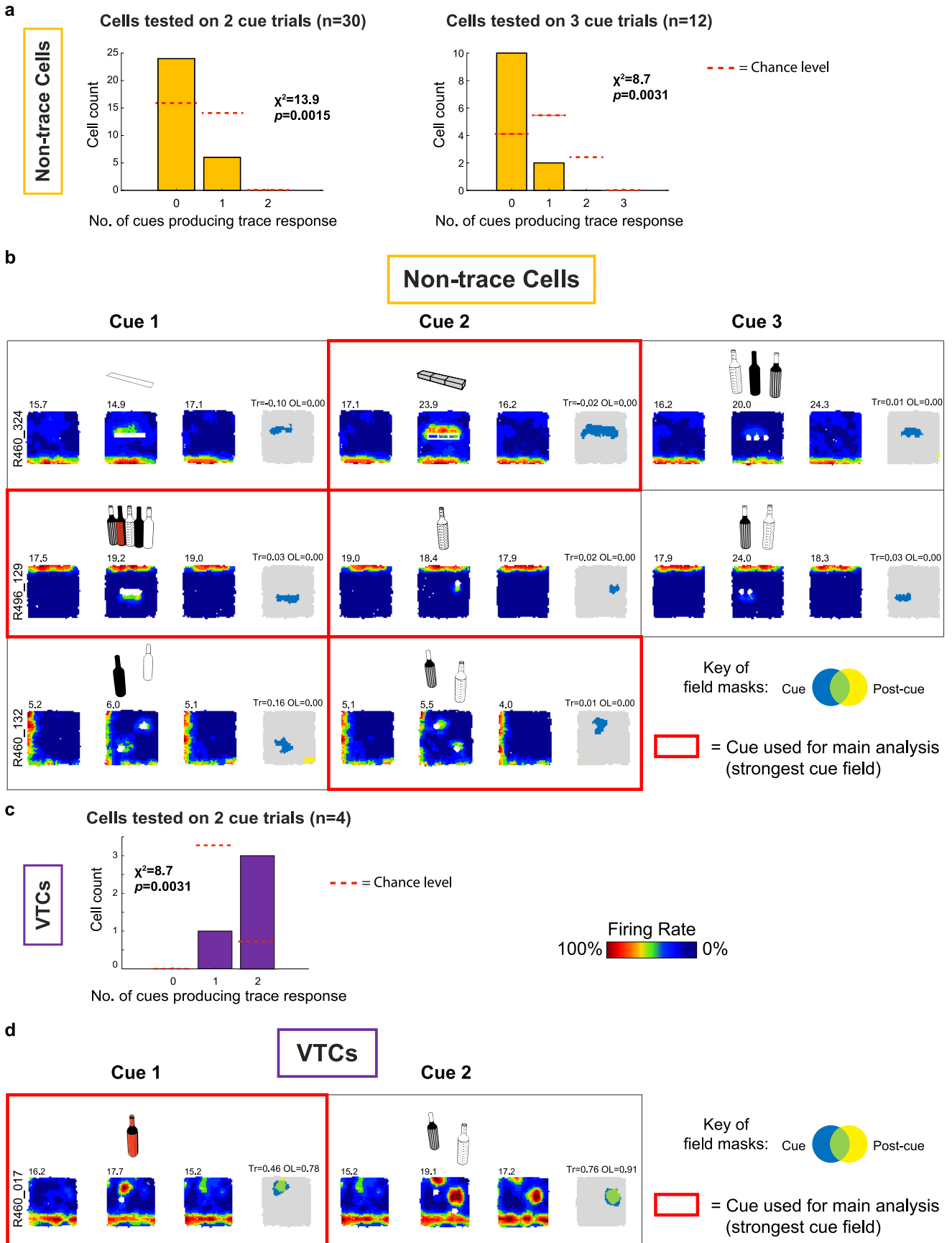
Peer review information *Nature Neuroscience* thanks Michael Hasselmo and the other, anonymous, reviewer(s) for their contribution to the peer review of this work.

Reprints and permissions information is available at www.nature.com/reprints.



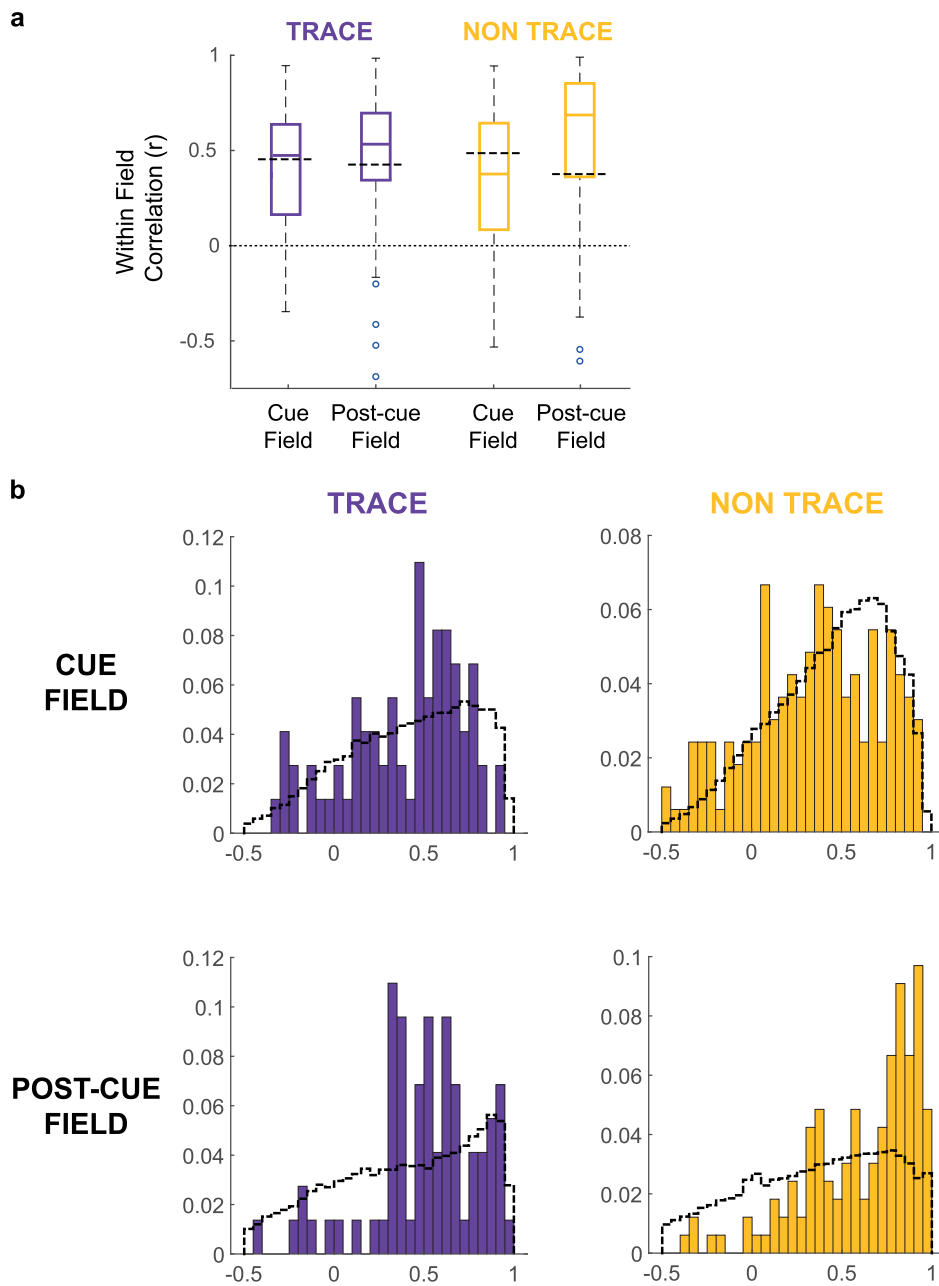
Extended Data Fig. 1 | See next page for caption.

Extended Data Fig. 1 | Co-recorded Vector Trace cells and Non-trace cells. Firing rate maps of simultaneously-recorded Vector Trace cells (VTC) and Non-trace cells in three rats. Conventions as in Fig. 1. Each row illustrates firing rate maps for one cell (peak-rate bin (Hz) top-left). Left column: Pre-cue trial. Left-middle column: Cue trial, where each cell forms a new firing field when the cue (white space) is introduced. Right-middle column: Post-cue trial. In VTCs (top row for each rat), following cue removal, the cue-responsive firing field persists. In contrast, in Non-trace cells, the cue-responsive firing field has diminished to below-threshold levels in the Post-cue trial. Right column: masks showing cue-responsive field (blue), post-cue field (yellow) and overlap between both (green). Trace (Tr) and overlap (OL) scores shown above each plot. Trace score value of non-trace cell R462_115 is 0.198, that is below Trace cell threshold of 0.20.

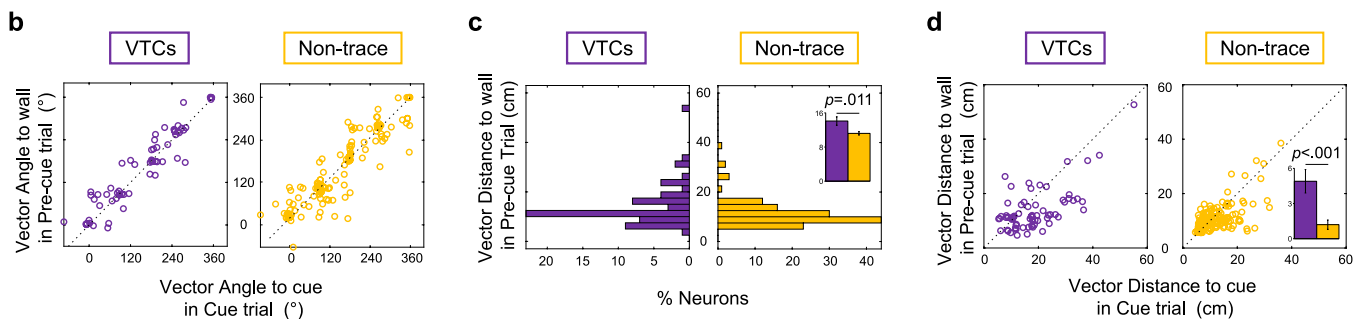
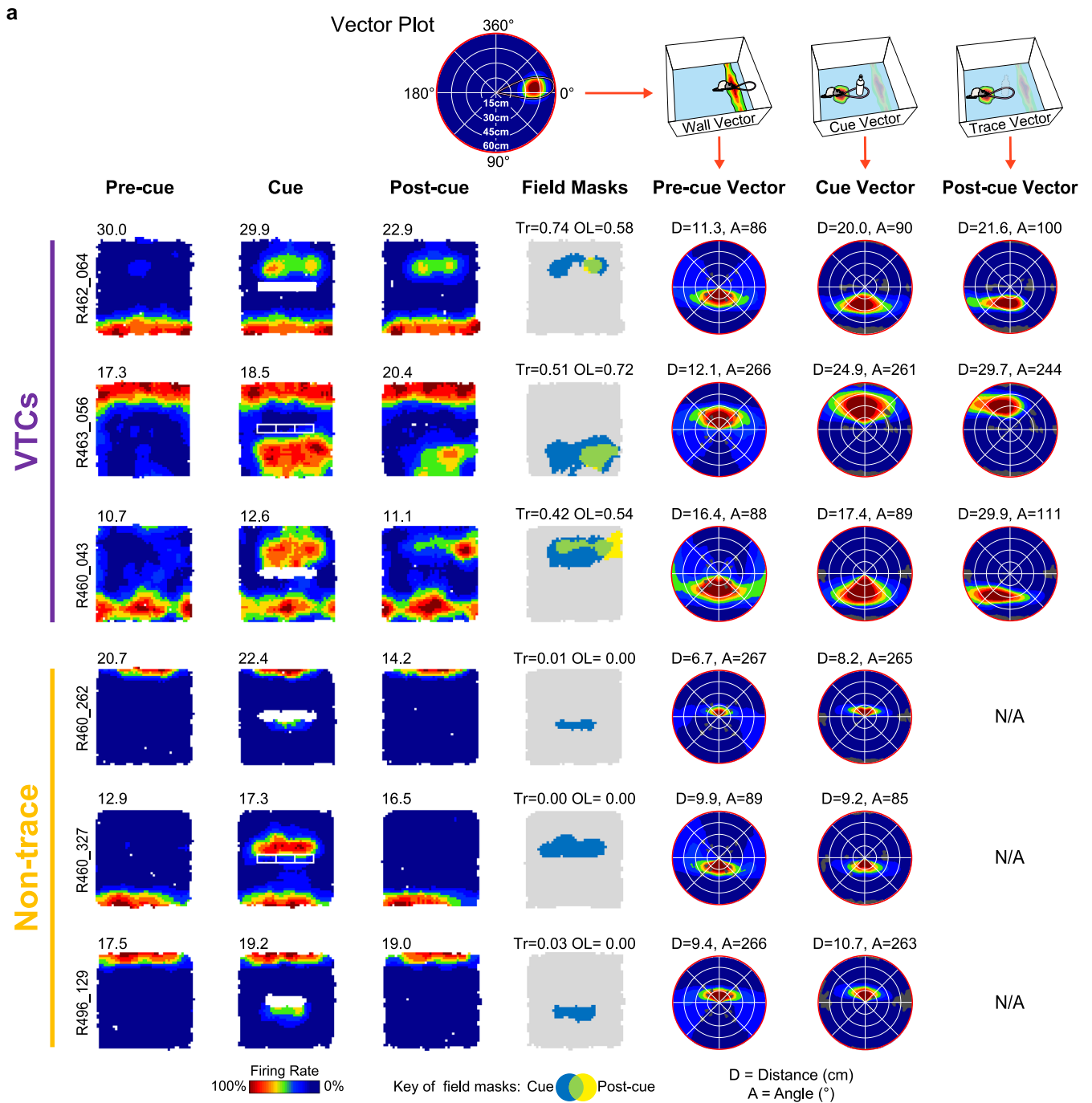


Extended Data Fig. 2 | See next page for caption.

Extended Data Fig. 2 | VTC and non-trace responses to multiple cue types. **a**, Occurrence frequency of trace responses across multiple cues, in non-trace cells. In the sub-set of cells exposed to multiple different cue trials in one experimental session, the cue that evoked the strongest cue field was used to classify the cell as VTC or non-trace (see Methods). Following this, the total number of cues which evoked a significant trace response was determined for each cell. Bar graphs in **(a)** show the numbers of non-trace cells exposed to two cue types (left) or three cue types (right) which were determined to show 0, 1 or 2 trace responses across the entire experimental session. (Data are split into 2-cue sessions vs 3-cue sessions to facilitate statistical testing). In both the two-cue and three-cue sessions, non-trace cells were significantly biased towards exhibiting fewer trace responses than expected by chance. Red dashed lines show chance levels, calculated under the assumption that, once a cell has been classified as non-trace on one trial, there is an independent 0.29/0.71 chance of observing a trace vs non-trace response for each further cue tested. (Chance levels equivalent to overall occurrence frequency of VTCs vs Non-trace cells amongst subiculum neurons). χ^2 tests were used to assess the significance of the difference between the observed frequencies and those expected under chance assumptions: χ^2 stats and significance levels are shown on the bar graphs (Y axis shows sample n). Note that chance levels are zero in the categories corresponding to trace responses occurring on all tested cues: non-trace cells must not exhibit a trace response on at least one cue by definition. **b**, Three example non-trace cells recorded across 3 cue trials (top two rows) or 2 cue trials (bottom row), which never showed a trace response. Rectangular boxes contain each cue trial set (that is Pre-cue, Cue, Post-cue trials) for each cue that a cell was exposed to. Note that the Post-cue trial for one cue forms the Pre-cue trial for following cue, hence rate maps are repeated across cue trial sets. Cue trial sets outlined in bold red were those with the strongest cue field response, which were used for cell type classification, and contributed to the main analysis. Cartoons above each cue trial show the type of cue used. Figure conventions in **(b)** as per Fig. 1. **c**, Occurrence frequency of trace responses across multiple cues, in VTCs. Only a small number of VTCs are available to test (N=4) due to proportionally lower sampling of VTCs in multiple-cue sessions, and to the long-lasting nature of the trace response: as the Post-cue trial of one cue formed the Pre-cue trial of the following cue, trace responses to earlier cues prevented detection of cue responses to later cues. Only 4 VTCs were recorded in which cue-evoked responses can be detected across two different cue types. In these cells, more VTCs than expected by chance exhibited a trace response on both cue types. Assumptions for generation of chance levels and methods of statistical testing for **(c)** were as for (A). **d**, One example VTC recorded across 2 cue trials, which showed a trace response on both cues. Black grid delineates each cue trial set (that is Pre-cue, Cue, Post-cue trials) for each cue run on each cell. Cue trial sets outlined in bold red were those with the strongest cue field response, which were used for cell type classification, and contributed to the main analysis. Cartoons above cue trial show the type of cue used.

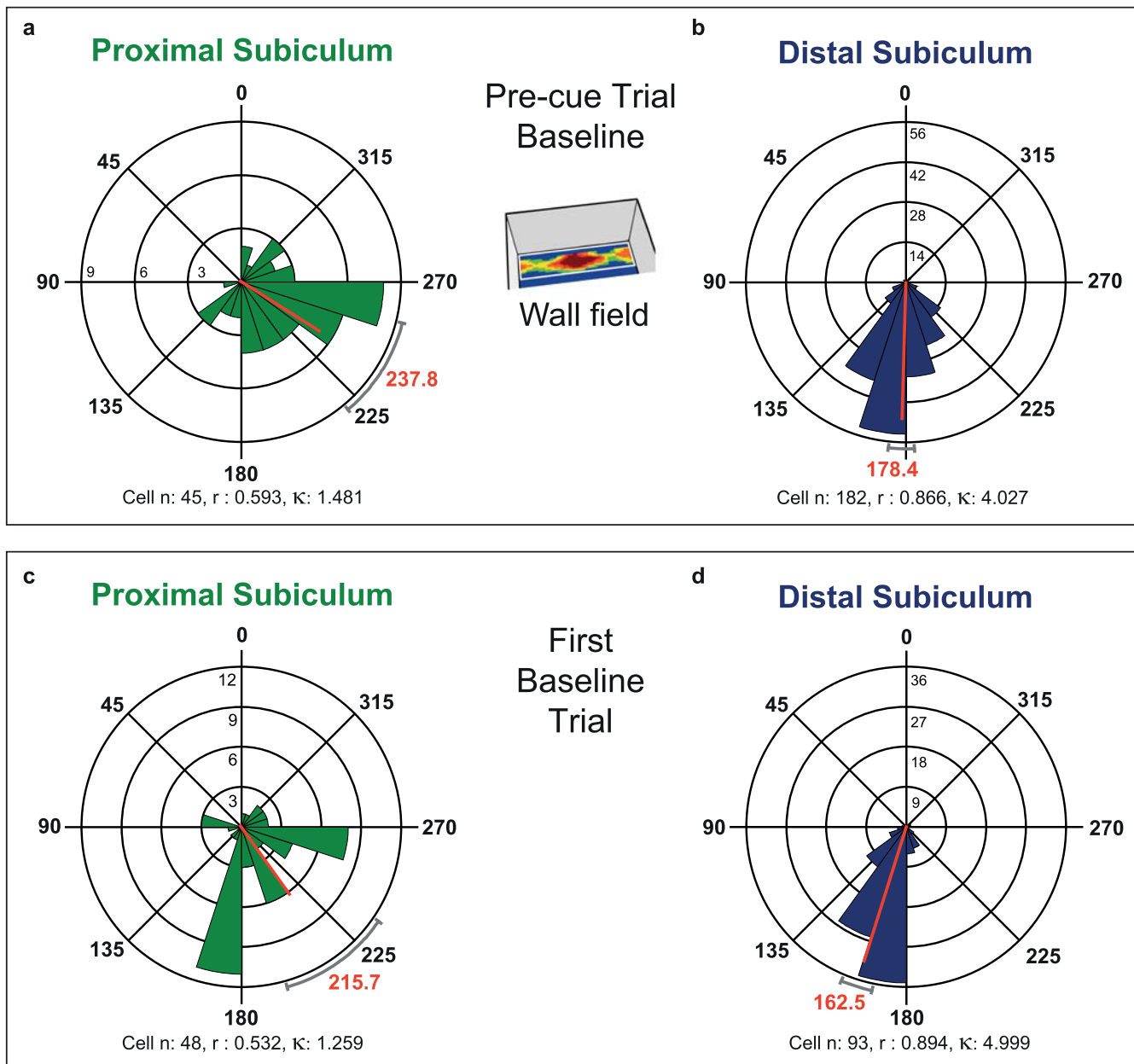


Extended Data Fig. 3 | Spatial firing in Pre-cue trial does not explain the position of trace fields in the Post-cue trial. **a**, Boxplots showing distributions of firing rate correlations across pre- and post-cue trials, restricted to those spatial bins within either the cue- or post-cue field. Boxes show 25th - 75th percentile, central line shows median. Whisker length is $IQR \times 1.5$, data points beyond whiskers are shown as individual points. All analyses in this Figure based on $n = 73$ VTCs and $n = 164$ Non-trace cells, using two-tailed t-tests. Non-trace cells in which a post-cue field could not be defined (no elevated area of firing in post-cue compared to pre-cue trial could be detected) were excluded from this analysis. The mean correlation for both fields and both cell types are significantly greater than zero (T-test, Fisher-transformed r : VTC cue field, $t_{72}=9.5$, $p < 0.00001$; VTC post-cue field, $t_{72}=9.7$, $p < 0.00001$; Non-trace cue field, $t_{163}=11.0$, $p < 0.00001$; Non-trace post-cue field, $t_{163}=15.8$, $p < 0.00001$), indicating that some spatial structure of neuronal firing in the pre-cue trial is conserved in the Post-cue trial (despite the emergence of a trace field, in VTCs). However, for VTCs, the correlation observed is not significantly greater than the mean of a population of correlations derived from spatially-randomised Cue- and Post-cue field positions (see Methods; T-test Fisher-transformed r versus mean of shuffled population: VTC cue field, $t_{72}=1.14$, $p = 0.26$; VTC Post-cue field, $t_{72}=1.65$, $p = 0.10$), demonstrating that the Cue- and Post-cue fields are not areas of enhanced similarity between the Pre- and Post-cue fields, compared to the remainder of the rate map (excluding the Wall field). Gray dashed lines show medians of spatially-randomised r populations. For non-trace cells, correlations were significantly lower than the mean of the spatially randomized population within the cue field ($t_{163} = 3.0$, $p = 0.003$), but significantly higher than the spatially randomized population in the post-cue field ($t_{163}=8.33$, $p < 0.00001$). **b**, Histograms showing the distributions underlying the box plots in (A). Colored bars show distributions of within-field correlations, grey dashed lines show the cell- and field type-matched distributions of spatially randomized field correlations.

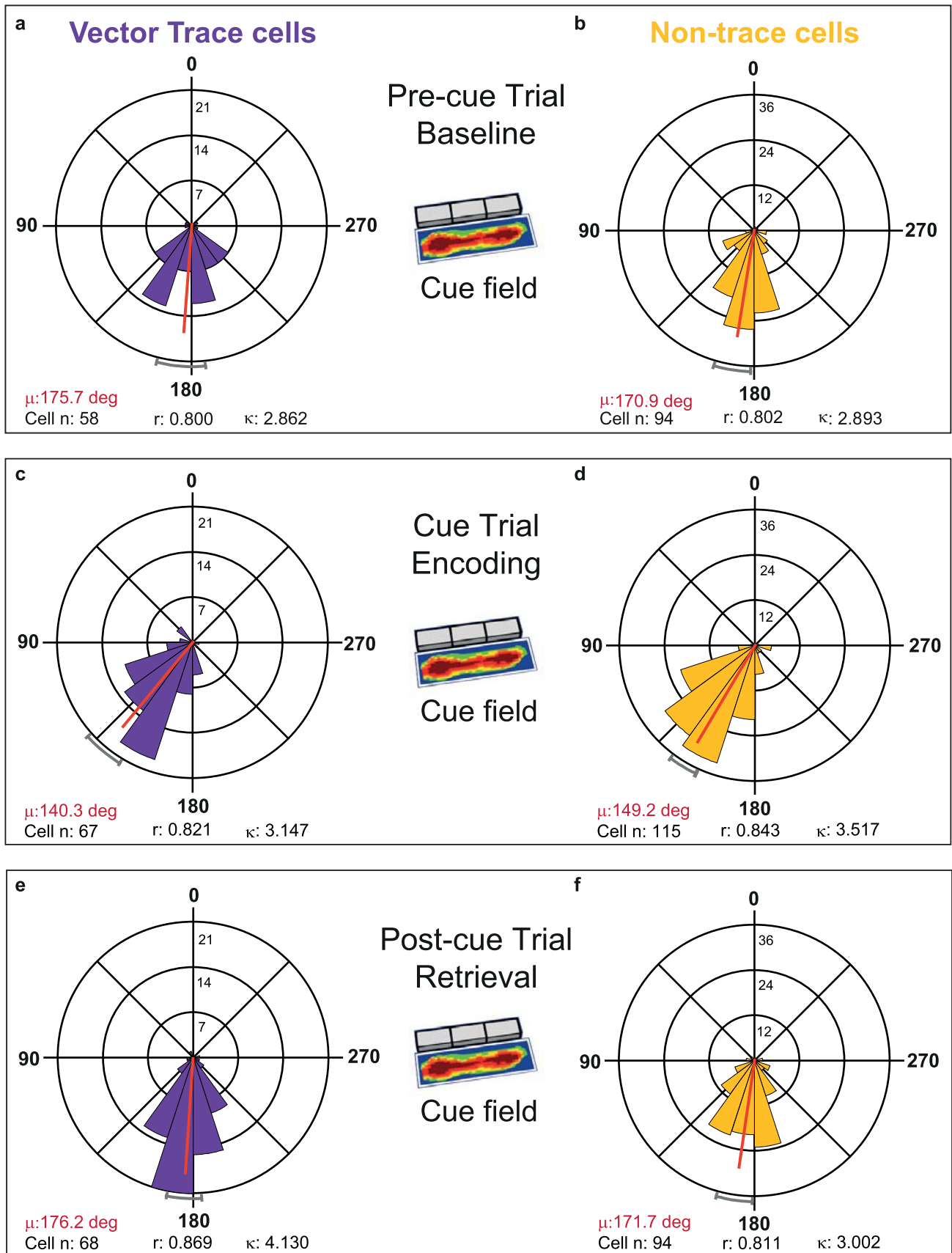


Extended Data Fig. 4 | See next page for caption.

Extended Data Fig. 4 | Analysis of wall vectors. Angular tunings between wall-field and cue-field vectors were similarly stable across VTCs and non-trace cells; VTCs' distance tunings showed more variance and were longer than those of non-trace cells; distance tunings were longer for cue fields than wall fields in both cell types, but this was more pronounced in VTCs. **a**, Rate maps and vector plots for three representative VTCs, and three representative non-trace cells. Conventions as Fig. 1a,b for first four columns. Conventions as Fig. 2a,b for columns of vector plots: wall field vector in Pre-cue trial (5th column); cue field vector in Cue trial (6th column); and trace field (cue) vector in the Post-cue trial (7th column). Distance tuning scale is 0–60cm in all vector plots. **b**, Scatterplots of angular tunings showing VTCs (left, $n=64$) and non-trace cells (right, $n=132$) showed stable angular tuning for wall-field vector in Pre-cue trial vs Cue-field vector in Cue trial. The overall mean angular difference between the wall-field and the cue field was $8.2 \pm 4.4^\circ$ (mean absolute angular difference: $26.2 \pm 3.3^\circ$) for VTCs, and $0.9 \pm 3.9^\circ$ (mean absolute angular difference: $32.5 \pm 3.0^\circ$) for Non-trace cells, with no difference between the cell types (Watson-Williams $F_{1,194} = 1.32$, $p = 0.25$; Welch $t_{194} = 1.416$, $p = 0.16$). For VTCs, the overall mean angular difference between the Pre-cue wall-field and the Post-cue trace field was similarly minimal at $4.1 \pm 4.4^\circ$ (mean absolute angular difference: $28.3 \pm 2.9^\circ$). Thus, as expected, angular tunings were stable across wall fields and cue fields. The inter-trial absolute difference values involving the wall field show somewhat larger error than those in VTCs between the cue field and its trace field ($19.5 \pm 2.7^\circ$, see Fig. 2e & main text), because square-walled environments are suboptimal for estimating angular orientation of vector fields⁵⁷. **c**, Histograms of distance tunings for VTCs (left) and Non-trace cells (right) for wall-field vector in Pre-cue trial. Exactly as for cue field vectors' distance tunings (main text, Fig. 2c), VTCs' distance tunings in their wall-field vectors showed a much wider variance than those of non-trace cells (F test variance ratio = 2.46, $p < 0.001$) and were longer than those of non-trace cells (Inset compares mean \pm s.e.m. values: VTCs $n=64$: 14.1 ± 1.0 cm; Non-trace $n=132$: 11.2 ± 0.4 cm; Welch $t_{194} = 2.605$; $p = 0.011$). **d**, Scatterplots of distance tunings for VTCs (left) and Non-trace cells (right) for wall-field vector in Pre-cue trial vs cue-field vector in Cue trial. Distance tunings were longer for cue field than wall field vectors in both cell types (VTCs: paired $t_{63} = 5.04$, $p < 0.0001$; Non-trace: paired $t_{131} = 2.76$, $p = 0.007$), and this lengthening effect was more pronounced in VTCs (Inset compares mean \pm s.e.m. values: VTCs $n=64$: $+4.9 \pm 1.0$ cm; Non-trace $n=132$: $+1.2 \pm 0.4$ cm; Welch $t_{194} = 3.435$, $p = 0.0009$). All linear tests in this Figure were 2-tailed.



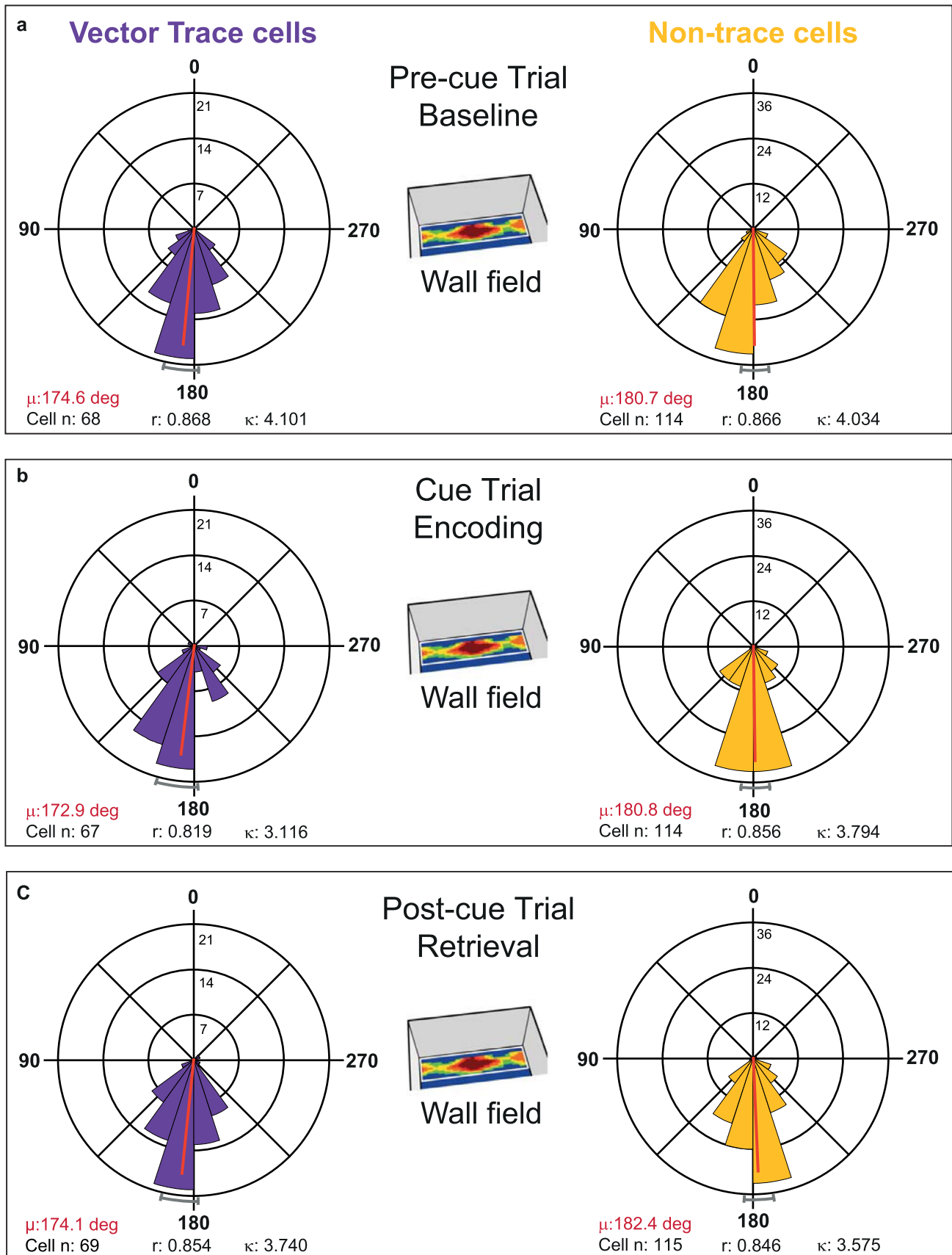
Extended Data Fig. 5 | Preferred theta phase of firing in the distal subiculum occurs around a sixth of a theta cycle earlier than in the proximal subiculum. a,b, Polar histograms showing distribution of individual cell phases of cue responsive cells in the wall field area in the Baseline (Pre-cue) trial in the proximal subiculum (**a**) and in the distal subiculum (**b**). Phase distribution is more concentrated in the distal subiculum, where mean preferred phase occurs a sixth-cycle earlier than in the proximal subiculum (59.4 degrees earlier: Watson-Williams F test for difference between means: $F_{1,225} = 68.50$, $p < 1 \times 10^{-12}$). **c,d**, Polar histograms showing distribution of individual cell phases for cells of all types (except cue-responsive cells above) in first baseline trial in the proximal subiculum (**c**) and in the distal subiculum (**d**). Similarly to cue-responsive cells, phase distribution is again more concentrated in the distal subiculum, and mean preferred phase occurs considerably earlier in the distal than proximal subiculum (53.2 degrees earlier: Watson-Williams F test for difference between means: $F_{1,139} = 40.11$, $p = 3.1 \times 10^{-9}$). Phases are divided into twenty 18-degree bins (0/360=peak;180=trough). Scale near 90-degree line (**a**), and zero-degree line (**b,c,d**) indicates number of cells in a given phase bin. Key: μ is mean phase (red line, red font text), r is length of Rayleigh vector (also indicated by length of red mean phase line, from centre to outer circumference), κ is Von Mises' κ (indexing phase concentration). Grey curved caps depict $\pm 95\%$ confidence limits. All phases are referenced to theta recorded from distal subiculum.



Extended Data Fig. 6 | See next page for caption.

Extended Data Fig. 6 | Preferred theta phase of firing shifts markedly earlier during cue-related encoding in both vector trace cells and non-trace cells.

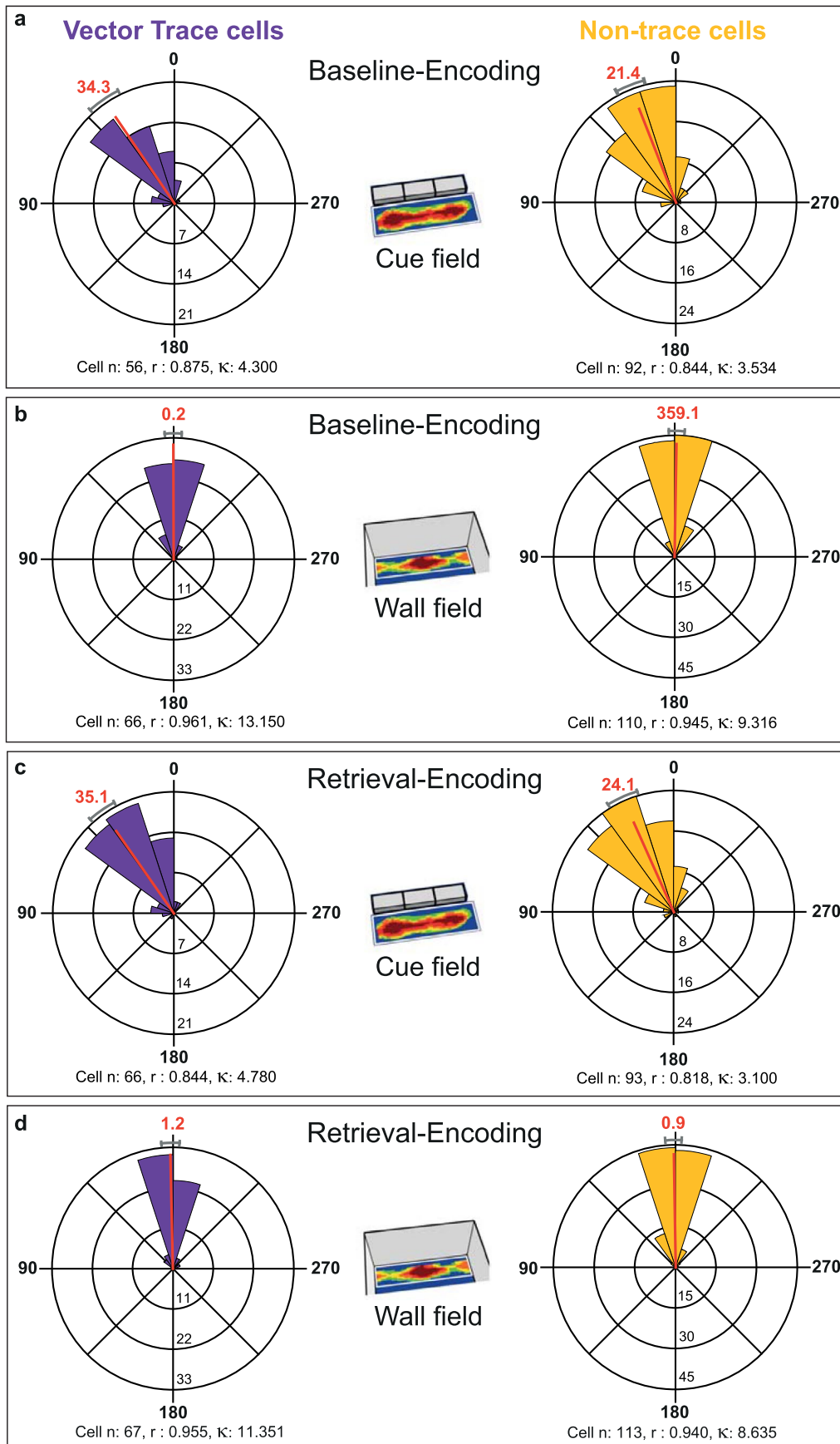
Polar histograms showing distribution of individual cell phases in the cue field area whose mean phases (red lines, red-font text) and 95% confidence limits (grey curved caps at perimeter) are shown in Fig. 6, for each of the two cell types: (a to b) trace cells, (e to f) non-trace cells, from Pre-cue trials (a,e), to Cue trials (c,d), to Post-cue trials (b,f). Preferred theta phase of firing is very stable across Pre-cue and Post-cue trials in both cell types. Notably, against this background of strong phase stability, preferred theta phase of firing is markedly earlier in both cell types during Encoding trials (Cue Trial: c,d) than during Baseline (Pre-cue Trial: a,e) and Retrieval (Post-cue Trial: b,f) trials (all Cue-vs-Pre-cue & Cue-vs-Post-cue F values >19.25, all p values < 1.82 x 10⁻⁵). Within-cell earlier shift in Encoding was greater in vector trace cells than non-trace cells (main text; Fig. 6) There were no within-trial, across-cell-type, absolute-phase differences (Watson-Williams F tests: Pre-cue trial: F_{1,150} = 0.55, p = 0.46; Cue-trial: F_{1,180} = 2.81, p = 0.10; Post-cue trial: F_{1,160} = 0.69, p = 0.41). Phases are divided into twenty 18-degree bins (0/360:peak,180:trough). Vertical scale near zero-degree line indicates number of cells in a given phase bin. Key: μ is mean phase (red line, red font text), r is length of Rayleigh vector (also indicated by length of red mean phase line, from centre to outer circumference), k is Von Mises' k (indexing phase concentration). Grey curved caps depict +/- 95% confidence limits.



Extended Data Fig. 7 | See next page for caption.

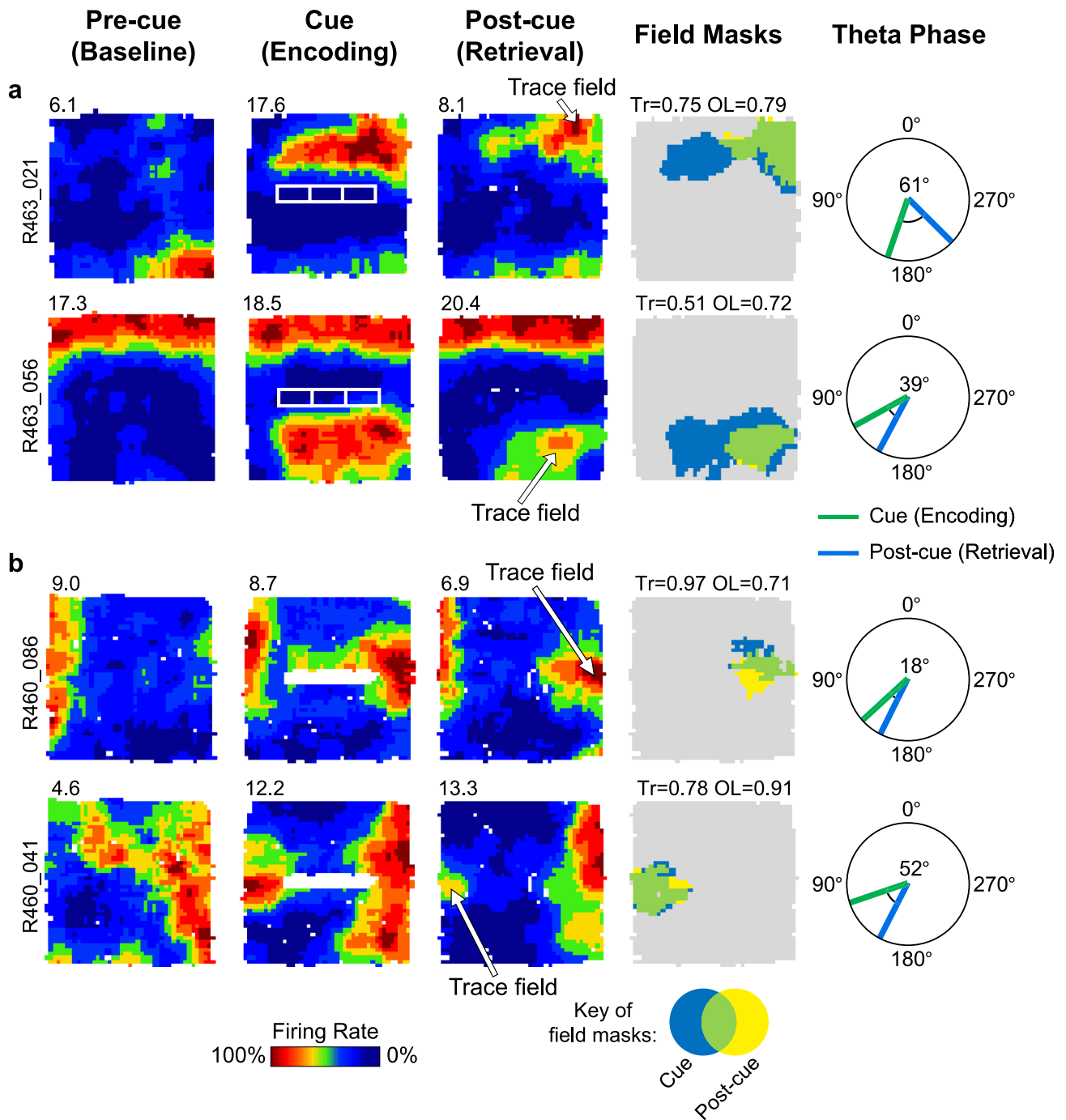
Extended Data Fig. 7 | Preferred theta phase of firing is highly stable across trials in the wall field in both vector trace cells and non-trace cells.h.

Polar histograms detailing distribution of individual cell phases in the wall field area whose mean phases (red lines, red-font text) and 95% confidence limits (grey curved caps at perimeter) are shown in Fig. 6b, for each of the two cell types: (left column) trace cells, (right column) non-trace cells, from Pre-cue trials (**a**), to Cue trials (**b**), to Post-cue trials (**c**). Across-trial preferred theta phase of firing is very stable (Watson-Williams F tests comparing within-cell-type, across-trial, phase distributions: $2 \times 3 = 6$ tests; all 6 test F values < 0.083 , all p values > 0.77). There were no within-trial, across-cell-type differences (Pre-cue; $F_{1,180} = 1.70$, $p = 0.19$; Cue: $F_{1,179} = 2.31$, $p = 0.13$; Post-cue: $F_{1,182} = 2.79$, $p = 0.10$). Phases are divided into twenty 18-degree bins (0/360=peak; 180=trough). Vertical scale near zero-degree line indicates number of cells in a given phase bin. Key: μ is mean phase (red line, red font text), r is length of Rayleigh vector (also indicated by length of red mean phase line, from centre to outer circumference), k is Von Mises' k (indexing phase concentration). Grey curved caps depict \pm 95% confidence limits.

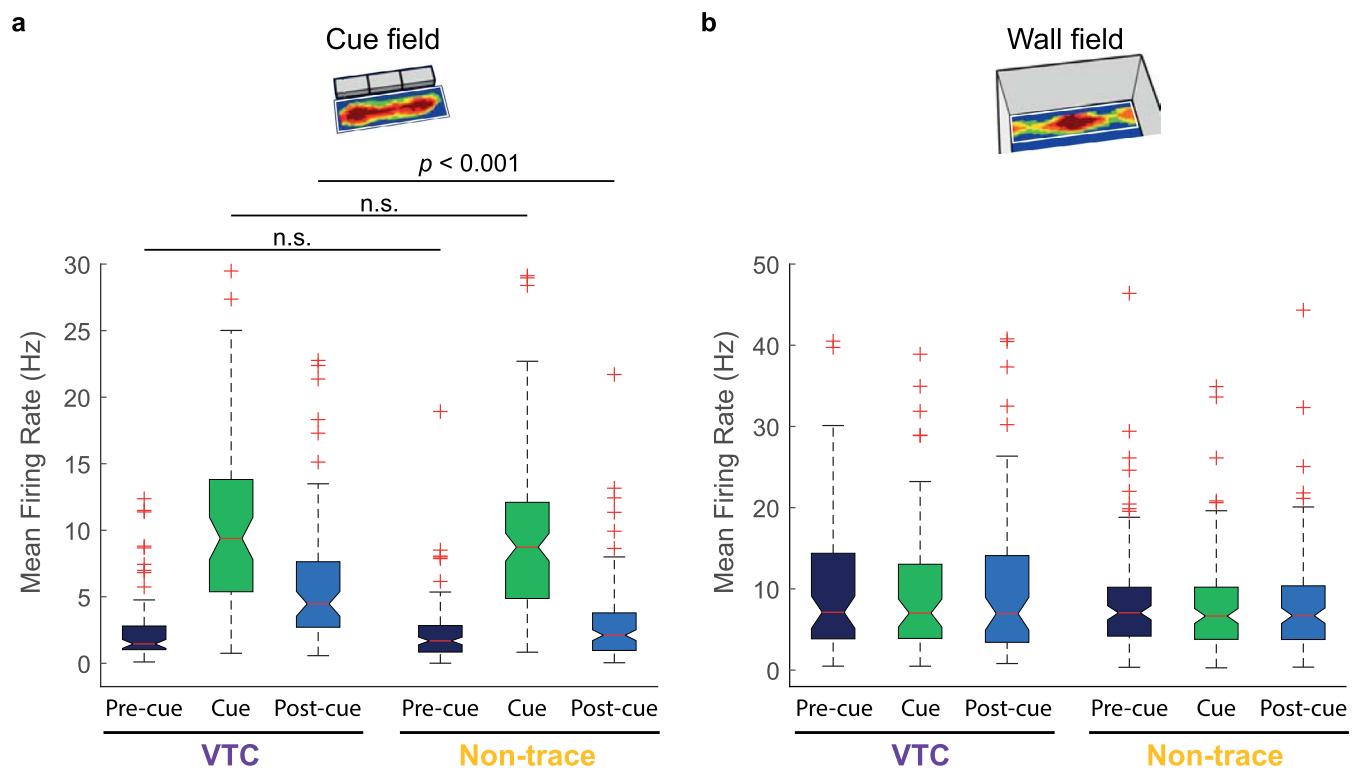


Extended Data Fig. 8 | See next page for caption.

Extended Data Fig. 8 | Earlier-going shift in theta phase preference in the cue field is larger in vector trace cells than non-trace cells. Polar histograms detailing distribution of phase difference data summarized in Fig. 6b for Baseline-Encoding comparisons (**a,b**) and Retrieval-Encoding comparisons (**c,d**) for VTCs (left column) and non-trace cells (right column). Differences are expressed as Precue-minus-Cue trial (Baseline-Encoding) and Postcue-minus-Cue trial (Retrieval-Encoding). The earlier-going phase shift in the cue field was larger in distal VTCs than distal non-trace cells, both for the baseline-vs-encoding comparison (**a**): Precue-Cue: Watson-Williams $F_{1,146} = 5.72$, $p = 0.018$, and the retrieval-vs-encoding comparison (**c**): Postcue-Cue: Watson-Williams $F_{1,157} = 4.29$, $p = 0.04$). In contrast, the baseline-vs-encoding (**b**) and retrieval-vs-encoding differences (D) in the wall field were similarly concentrated near zero for both VTCs and non-trace cells (Precue-Cue (B): Watson-Williams $F_{1,174} = 0.17$, $p = 0.68$; Postcue-Cue (**d**): Watson-Williams $F_{1,178} = 0.01$, $p = 0.92$). Note appreciably higher concentrations of phase (indexed by Von Mises' k) around the zero-difference values in wall fields than cue fields in both cell types, indicative of stability of theta phase in the wall field. Phases are divided into twenty 18-degree bins (0/360=peak; 180=trough). Vertical scale near 180-degree line indicates number of cells in a given phase bin. Key: μ is mean phase (red line, red font text), r is length of Rayleigh vector (also indicated by length of red mean phase line, from centre to outer circumference), k is Von Mises' k (indexing phase concentration). Grey curved caps depict +/- 95% confidence limits.



Extended Data Fig. 9 | Examples of simultaneously-recorded vector trace cell pairs, demonstrating phase changes are specific to cue-driven firing, and not linked to one region in the recording arena. a, b. Simultaneously-recorded pairs of vector trace cells in two rats. Columns left to right: rate maps for each cell across trials (Pre-cue, Cue, Post-cue), field masks (Cue and Post-cue), and preferred (mean) theta phase of firing in Encoding and Retrieval trials ('Theta phase in cue field region'). These examples show that the same cue (A: 4.5cm high brick array; B: 50cm high wall) elicits, in simultaneously-recorded cells, trace fields occupying different areas of the box, far from each other. VTC firing at earlier theta phase is specifically linked to the cue-driven firing field for each cell, and, across cells, is dissociated from the rat's position.



Extended Data Fig. 10 | Firing rates in VTC and non-trace cells in distal subiculum can be dissociated from phase. Boxplots showing distributions of mean neuronal firing rates in the cue field (**a**) and wall field (**b**), in both VTCs and Non-trace cells in distal subiculum. Boxes show 25th - 75th percentile, central line shows median. Whisker length is IQR \times 1.5, data points beyond whiskers are shown as individual points. One possible account of changes in preferred phase (for example following cue insertion), is that these may reflect high-rate and low-rate regimes of firing respectively, under models of theta phase precession in which higher depolarisation drives earlier phase of firing^{68,69} butsee⁷⁰. Here we show that, by contrast, phase and firing rate can be dissociated, in particular in the Post-cue trial. Consistent with our cell-type classifications, VTC firing rates were significantly greater than Non-trace cell firing rates in the cue field area in the Post-cue trial (A: 2-way mixed ANOVA cue field firing rates: Trial \times Cell type; $F_{2,284} = 8.1$, $p < 0.001$; Post hoc Simple Main Effects VTC vs Non-trace: Pre, $p = 0.63$; Cue, $p = 0.137$; Post, $p < 0.001$. N Cells = 56 VTCs, 88 Non-trace cells. Cells were filtered as for phase analyses: cells without theta modulation [Rayleigh $p > 0.01$] or < 50 spikes in cue field were excluded). By contrast, there was no difference in the preferred phase of VTC and Non-trace cells, in any trial, including the Post-cue trial (see Fig. 6, Extended Data Fig. 6, Watson-Williams F tests: Pre-cue trial: $F_{1,150} = 0.55$, $p = 0.46$; Cue-trial: $F_{1,180} = 2.81$, $p = 0.10$; Post-cue trial: $F_{1,160} = 0.69$, $p = 0.41$). There is therefore no significant difference between VTCs and Non-trace firing rate in the cue trial which could explain the greater earlier-going phase shift. Furthermore, there is a strong dissociation between phase and rate in the Post-cue trial, whereby VTC rates are significantly higher than Non-trace cell rates, but preferred phase is strongly similar for the two classes of neuron. We note that, even in Non-trace cells, firing rates in the cue field increase between the Pre- and Post-cue trials (Simple Main Effects, $p = 0.005$), possibly due to imperfect classification of VTC versus Non-trace cells, or due to some residual memory-based firing occurring even in non-trace cells. In the wall field (**b**), VTCs showed significantly greater firing rates overall (2-way mixed ANOVA wall field firing rates: Trial; $F_{2,352} = 6.9$, $p = 0.001$), but no cell-type specific changes in firing across trials (Trial \times Cell type; $F_{2,352} = 0.65$, $p = 0.52$. N Cells = 66 VTCs, 112 non-trace cells. Cells were filtered as for phase analyses: cells without theta modulation [Rayleigh $p > 0.01$] or < 50 spikes in wall field were excluded). All linear tests in this Figure were 2-tailed.

Reporting Summary

Nature Research wishes to improve the reproducibility of the work that we publish. This form provides structure for consistency and transparency in reporting. For further information on Nature Research policies, see our [Editorial Policies](#) and the [Editorial Policy Checklist](#).

Statistics

For all statistical analyses, confirm that the following items are present in the figure legend, table legend, main text, or Methods section.

- | | |
|-----|-----------|
| n/a | Confirmed |
|-----|-----------|
- The exact sample size (n) for each experimental group/condition, given as a discrete number and unit of measurement
 - A statement on whether measurements were taken from distinct samples or whether the same sample was measured repeatedly
 - The statistical test(s) used AND whether they are one- or two-sided
Only common tests should be described solely by name; describe more complex techniques in the Methods section.
 - A description of all covariates tested
 - A description of any assumptions or corrections, such as tests of normality and adjustment for multiple comparisons
 - A full description of the statistical parameters including central tendency (e.g. means) or other basic estimates (e.g. regression coefficient) AND variation (e.g. standard deviation) or associated estimates of uncertainty (e.g. confidence intervals)
 - For null hypothesis testing, the test statistic (e.g. F , t , r) with confidence intervals, effect sizes, degrees of freedom and P value noted
Give P values as exact values whenever suitable.
 - For Bayesian analysis, information on the choice of priors and Markov chain Monte Carlo settings
 - For hierarchical and complex designs, identification of the appropriate level for tests and full reporting of outcomes
 - Estimates of effect sizes (e.g. Cohen's d , Pearson's r), indicating how they were calculated

Our web collection on [statistics for biologists](#) contains articles on many of the points above.

Software and code

Policy information about [availability of computer code](#)

Data collection

Electrophysiological Data Collection:
Axona DACQ USB (version 1.3)

Images of coronal brain sections:

Adobe Photoshop Express 3.5 for conversion of colour photomicrographs to black and white, and adjustment of contrast and brightness.

Data analysis

For Electrophysiological Data:

Axona TINT (version 4.4) and Klustakwik (Version 3) for isolation of cell clusters.

Custom written Matlab Scripts for generation of and analysis of positional rate maps and associated variables (Trace score, Overlap, Vector displacement firing rate maps giving angular tuning and distance tuning, across-trial and within-trial spatial bin-by-bin correlation, shuffling procedures).

Custom written Matlab scripts for statistical analysis of chance occurrence of trace response (Chi-squared test) and of spatial bin-by-bin correlation (Fisher-transformed t test).

Custom written Matlab Scripts for analysis of theta power (fast-fourier transform).

Custom written Matlab scripts for extraction of theta phase of spiking, analysis of meeting thresholds for theta modulation (Rayleigh $p < 0.01$) and spike count (50 spikes), and then provision of cellular Rayleigh r values and cellular mean phase values for analysis in Oriana;

Oriana (Version 4, Kovach Computing), to derive values for circular-statistics related variables:

Rayleigh vector r tests, Von Mises K , 95% confidence intervals [figures], circular standard error of mean [main text], Watson-Williams F tests, Watson's U^2 test, Kuiper's V test.

Medcalc (version 19.4.0) for analyses of distance tunings and theta modulation of spiking (t-tests, Welch t-tests, Variance Ratio test).

IBM SPSS 23 for ANOVA analysis of firing rates and speed-filtered intra-trial spatial correlations.

For manuscripts utilizing custom algorithms or software that are central to the research but not yet described in published literature, software must be made available to editors and reviewers. We strongly encourage code deposition in a community repository (e.g. GitHub). See the Nature Research [guidelines for submitting code & software](#) for further information.

Data

Policy information about [availability of data](#)

All manuscripts must include a [data availability statement](#). This statement should provide the following information, where applicable:

- Accession codes, unique identifiers, or web links for publicly available datasets
- A list of figures that have associated raw data
- A description of any restrictions on data availability

Provide your data availability statement here.

Field-specific reporting

Please select the one below that is the best fit for your research. If you are not sure, read the appropriate sections before making your selection.

Life sciences Behavioural & social sciences Ecological, evolutionary & environmental sciences

For a reference copy of the document with all sections, see nature.com/documents/nr-reporting-summary-flat.pdf

Life sciences study design

All studies must disclose on these points even when the disclosure is negative.

Sample size	No statistical methods were used to pre-determine sample sizes (cell numbers). All available sessions where cue responsive cells were present and thus vector trace cells could have been observed (i.e. precue/cue/postcue trial series) were analysed. Our sample sizes were similar to sample sizes reported in previous publications [Refs 12,24,33-37].
Data exclusions	Data from non-locomotion periods (defined as movement speed < 5cm/s) were excluded from rate maps and theta phase of spiking data. This common filtering practice aims to restrict analysis to theta epochs and exclude firing from sharp-wave ripple epochs from the data. Supplementary Figure S1 shows spatial stability analyses when this exclusion was not applied. For theta phase of spiking analyses, further to movement speed filtering mentioned above, cells had to have a minimum of 50 spikes and show statistically significant (Rayleigh $p < 0.01$) theta modulation. These exclusion criteria were not pre-established, but follow (Jones and Wilson, PLOS Biology, 2005; Mizuseki et al, Neuron, 2009; Mizuseki et al, Nature Neuroscience, 2011; [ie Refs 64-66]; Mizuseki et al, Hippocampus, 2012). This common practice aims to reduce the influence of noisy data.
Replication	There were no separate replication experiments. Reproducibility was inferred by the observation of vector trace cells in the distal subiculum of each of the six rats tested, with mean per-rat proportion (35%; breakdown 17% (3/17); 29% (20/68); 33% (2/6); 36% (15/42); 47% (8/17); 50% (21/42)) similar to total proportion (36%, shown in Figure 5B). Not all Subicular cue-responsive cell ensembles contained VTCs. However, some ensembles contained just one or two cue-responsive cells, and/or sampled only from proximal subiculum, where (as described in the manuscript: main text & Figure 5) VTCs are rare.
Randomization	Randomization was not required as the study did not allocate different rat groups. Cues were varied (see Methods) but there was no formal randomization in the organization of stimulus presentations.
Blinding	Blinding to group was not required as the study did not allocate different rat groups. Data collection and analysis was not performed blinded to the conditions of the experiments.

Reporting for specific materials, systems and methods

We require information from authors about some types of materials, experimental systems and methods used in many studies. Here, indicate whether each material, system or method listed is relevant to your study. If you are not sure if a list item applies to your research, read the appropriate section before selecting a response.

Materials & experimental systems

Methods

- n/a Involved in the study
- Antibodies
- Eukaryotic cell lines
- Palaeontology and archaeology
- Animals and other organisms
- Human research participants
- Clinical data
- Dual use research of concern

- n/a Involved in the study
- ChIP-seq
- Flow cytometry
- MRI-based neuroimaging

Animals and other organisms

Policy information about [studies involving animals](#); [ARRIVE guidelines](#) recommended for reporting animal research

Laboratory animals

Six Lister-Hooded male rats weighing approximately 392-522g and aged 3-5 months at the start of the experiment were used. Prior to surgery, they were housed in groups of four and after surgery housed individually at a temperature of 20-22 degrees C, humidity of 40-60%, and under a 12/12h light/dark (with lights off at 10am and all animals tested during their dark phase). After rats had recovered from surgery, food deprivation was maintained during recording periods such that subjects weighed 85-90% of free feeding weight.

Wild animals

No wild animals were used.

Field-collected samples

No field collected samples were used.

Ethics oversight

Approval for the animal experiments was granted by both Durham University AWERB and United Kingdom Home Office Project and Personal Licenses.

Note that full information on the approval of the study protocol must also be provided in the manuscript.